FINAL REPORT FOR CONTRACT **FA8655-04-1-3050**

Analysis of Conformal Stacked-Patch Arrays

by

Zvonimir Sipus
Sinisa Skokic
Niksa Burum

SUBMITTED BY: Dr. Zvonimir Sipus
Faculty of Electrical Engineering and Computing
University of Zagreb
Unska 3
Zagreb, HR-10000, Croatia

31 July 2005

20060414064

REPORT DOCUMENTATION PAGE

Form Approved OMB No. 0704-0188

1. REPORT DATE (DD-MM-YYYY) 13-09-2005	2. REPORT TYPE Final Report	3. DATES COVERED (From – To) 1 August 2004 - 01-Aug-05

4. TITLE AND SUBTITLE	5a. CONTRACT NUMBER
Analysis of Conformal Stacked-Patch Arrays	FA8655-04-1-3050
	5b. GRANT NUMBER
	5c. PROGRAM ELEMENT NUMBER

6. AUTHOR(S)	5d. PROJECT NUMBER
Professor Zvonimir Sipus	
	5d. TASK NUMBER
	5e. WORK UNIT NUMBER

7. PERFORMING ORGANIZATION NAME(S) AND ADDRESS(ES) University of Zagreb Unska 3 Zagreb HR-10000 Croatia	8. PERFORMING ORGANIZATION REPORT NUMBER N/A

9. SPONSORING/MONITORING AGENCY NAME(S) AND ADDRESS(ES) EOARD PSC 802 BOX 14 FPO 09499-0014	10. SPONSOR/MONITOR'S ACRONYM(S)
	11. SPONSOR/MONITOR'S REPORT NUMBER(S) SPC 04-3050

12. DISTRIBUTION/AVAILABILITY STATEMENT

Approved for public release; distribution is unlimited.

13. SUPPLEMENTARY NOTES

14. ABSTRACT

Formulation of the problem.   Modeling single circular stacked-patch antenna on spherical structures.   Modeling patch arrays on spherical structures. Development of experimental model.

15. SUBJECT TERMS
EOARD, Conformal Array Antennas, Antennas

16. SECURITY CLASSIFICATION OF:			17. LIMITATION OF ABSTRACT UL	18, NUMBER OF PAGES	19a. NAME OF RESPONSIBLE PERSON MICHAEL KJ MILLIGAN, Lt Col, USAF
a. REPORT UNCLAS	b. ABSTRACT UNCLAS	c. THIS PAGE UNCLAS		87	19b. TELEPHONE NUMBER (Include area code) +44 (0)20 7514 4955

Standard Form 298 (Rev. 8/98)
Prescribed by ANSI Std. Z39-18

TABLE OF CONTENTS

1   INTRODUCTION

Introduction

Rapid growth in wireless communications has caused that the requirements on antenna systems are more and more demanding. For example, future antenna systems will have a variety of beamforming and beamsteering capabilities, and they will be integrated in the surfaces of different vehicles or platforms. In order to ensure proper operation of the communication system it is important to be able to determine the characteristics of these antennas.

In the IEC International Electrotechnical Vocabulary, a *conformal antenna* is defined as: *An antenna which conforms to a surface whose shape is mainly determined by considerations other than electromagnetic, e.g. aerodynamic or hydrodynamic considerations.* In other words, conformal antennas can be mounted on various airborne objects (fighter jets, smart missiles, rockets) without disturbing their aerodynamical properties. This definition should be broadened with antennas whose shape is not planar and is determined with specific electromagnetic reasons like coverage requirements. For example, arrays on cylindrical structures offer a possibility either to create directed beams in arbitrary direction in horizontal plane, or to create an omnidirectional pattern. Spherical arrays have the capability of directing single or multiple beams through a complete hemisphere. Therefore, spherical arrays are a good candidate for satellite terminals, telemetry and command applications, performed from a ground station.

One possible approach to analyzing conformal antennas is to approximate the conformal structure with a locally planar one, and then to apply some method for planar antennas. This is a reasonable approximation if the radius of the structure curvature is very large. However, for smaller radii the properties of the antenna begin to differ significantly from their planar counterpart and therefore the antenna shape should be rigorously taken into account. Additionally, in case of array applications, it is critical to be able to take into account the mutual coupling between the array elements. Mutual coupling can cause a significant change in element pattern of array elements, and therefore it must be included in the design procedure.

The purpose of this project is to develop a computer program that performs a rigorous analysis of spherical arrays of stacked-patch elements. For example, the multilayer spherical structure is taken into account by using proper Green's functions, and the array is analyzed by applying the moment method (element-by element approach) to determine the current distribution and in this way to determine the mutual coupling effects. The developed program can calculate all-important

information about the antenna array: the input port impedance, radiation pattern as well as the mutual coupling coefficients. The capabilities and accuracy of the computer program are tested on different practical designs found in scientific literature.

2 PROBLEM IDENTIFICATION
AND ITS SIGNIFICANCE

Problem Identification and its Significance

Spherical arrays present a natural choice if complete hemispherical coverage with nearly constant beam width is needed. The advantages of using spherical arrays for satellite tracking, telemetry and command applications, performed from ground stations, have been discussed recently [1]. The antenna elements are usually distributed following the icosahedron geometry, resulting in a good uniformity of element spacing [2]. Microstrip patch antennas can be easily made to conform to the structure and they are often used because of their thin profile, light weight and low cost. Therefore, one possible and simple realization of a spherical array is to use patch elements on a spherical supporting structure.

One possibility of analyzing a conformal array is to approximate it with a corresponding planar structure when calculating the element pattern, and to include the spherical array geometry by an appropriate coordinate and phase transformation. However, for most practical conformal antennas we cannot neglect the curvature of the structure, in particular when accounting for the mutual coupling effects since the magnitudes of the mutual coupling coefficients depend strongly on the structure curvature. Mutual coupling effects can drastically change the embedded element pattern of each antenna element, and therefore it is important to include them into the analysis procedure. The purpose of this paper is to present a rigorous analysis method for spherical arrays of patch elements.

Recently, there has been much progress in the theoretical analysis of conformal antennas. Most attention was given to circular-cylindrical antennas, probably due to varieties of applications where they can be used. They have been successfully analyzed using simple models like the cavity model [3], or using the full wave analysis (i.e. spectral-domain approach) [4]-[6]. Patch antennas on cylindrical structures with arbitrary cross-section have also been analyzed using spectral-domain approach [7]. General methods like FEM or FDTD have also been applied to different conformal antennas (see e.g. [8], [9]). However, a specific analysis method suitable for a particular type of conformal antenna is usually advantageous in terms of needed computer time. Therefore such a model is usually applied to investigate fundamental properties of conformal antennas and to obtain the first design of some particular antenna.

Spherical patch antennas are rarely considered in scientific literature. Previously, spherical patch antennas have been analyzed by applying the full wave spectral-domain method [10]-[12], cavity method [13], or generalized transmission-line method [14]. In all cases a single spherical patch with circular or annular-ring shape was analyzed (state of art about this subject can be found e.g.

in recently published book [15]). In other words, no results about the mutual coupling between microstrip antennas on spherical structures, or about the analysis of spherical stacked-patch antennas, are available in the open literature. The first effort in this direction was supported by the project F61775-01-WE024 where the arrays of single-layer rectangular microstrip patches mounted on spherical structures were fully analyzed (the main results following from that project were published in [16]-[18]). The proposed project covers the extension of the analysis method to stacked-patch antennas, in particular to circular patch antennas.

3 PROJECT OBJECTIVE AND REALIZED OUTCOMES

Project objective and realized outcomes

We proposed a 12-month effort to develop software for analyzing circular stacked-patch arrays mounted on double-curved structures. It was planned that the developed program would calculate the following antenna characteristics: (a) input impedance of each stacked-patch antenna in the array, (b) mutual coupling between each two patches in the array, (c) radiation pattern of the array. The project is a continuation and an upgrade of the program "SMiPA" that analyzes rectangular microstrip patch arrays placed on spherical structures (the program "SMiPA" is developed under project F61775-01-WE024).

During the first 6-months phase we have developed:

- The first version of the program "SMiSPA" that analyzes stacked-patch arrays printed on spherical structures. The patches are of circular shape, and they can be fed by a microstrip or coaxial transmission line. The program calculates:
  - o current distribution at each patch in the array
  - o input impedance at each input port in the array
  - o mutual coupling between each two patches in the array
  - o radiation pattern of the array when all mutual couplings are taken into account
  - o radiation pattern of the array without taking mutual coupling into account (fast calculations of the radiation pattern are needed for making first design of the array).

During the second 6-months phase we have improved the program SMiSPA. In more details, we have made:

- Investigation of the optimal choice of basis and test functions.

- Better model of the feeding coaxial probe. For that purpose a special attachment mode is added to the solution procedure, i.e. the values of input impedance and mutual coupling are determined more accurately.

- Experimental model by which different configurations of spherical stacked-patch antennas are investigated and the developed program validated.

The developed programs are written in FORTRAN program language since there is no faster programming language for computational physics (computational electromagnetics). The program is independent of the machine, and can be compiled and run on every machine that has a FORTRAN 90 compiler. Furthermore, for MS Windows PC environment, a graphical user interface is developed to allow for easier setting of input parameters, and to obtain graphical presentation of the results. On other machines or operating systems communication with the program is made via input/output ASCII files. In more details, the input file should be filled before running the program, and the results are written into the output file that can be graphically presented by any graphical program.

4   PROJECT OUTCOMES

4.1 Analysis of microstrip patch antennas
on spherical structures

4.1.1 Introduction

The purpose of this chapter is to describe the moment method analysis of spherical arrays of microstrip patch antennas embedded in a general multilayer spherical structure. The solution procedure takes advantage of the spectral-domain approach where a three-dimensional problem is transformed into a discrete spectrum of much simpler one-dimensional problems. In Section 4.1.2 we will give a brief description of the analysis method (more details can be found in [19]), while specific parts concerning circular stacked patch elements will be described in Sections 4.1.4 and 4.1.5.

4.1.2 Method of Analysis

The geometry of the problem is given in Figs. 4.1 and 4.2. An array of circular stacked-patches is embedded in a multilayer spherical structure. The radii of the grounded sphere, the fed patch and the parasitic patch are r_{gnd}, r_{patch_1} and r_{patch_2}, respectively. The coordinates of the central patch are $0 \leq \theta \leq \theta_{patch\_i}$ and $-\pi \leq \phi \leq \pi$ (θ_{patch_i} is defined as $\theta_{patch\_i} = r_i / r_{patch\_i}$, $i = 1, 2$). In other words, the center of the central patch is defined with $\theta = 0$. Other patch antennas have the same dimensions and their position can be obtained by rotating the central patch around the sphere center (notice that there is no simple expression for the coordinates of the edge of a generally positioned patch). The patch is fed by a coaxial transmission line, and the angular coordinates of the feeding point of the central patch center are θ_{feed} and ϕ_{feed}, respectively. Since the radius and the height of the probe are usually a small fraction of the wavelength, the probe is modeled as a filament of constant current.

The unknown patch current $\mathbf{J}(\theta, \phi)$ is expanded into a sum of entire domain basis functions $\mathbf{J}_i(\theta, \phi)$ (i.e. $\mathbf{J}(\theta, \phi) = \sum_i I_i \mathbf{J}_i(\theta, \phi)$) and the unknown amplitudes I_i are determined by applying the moment method (MoM) – Galerkin's approach. The solution procedure makes use of the spectral domain technique where a three-dimensional problem is transformed into a spectrum of one-dimensional problems. Since the problem is defined in the spherical coordinate system this spectrum is obtained by applying the vector-Legendre transformation to the patch current. [10], [19], [20]:
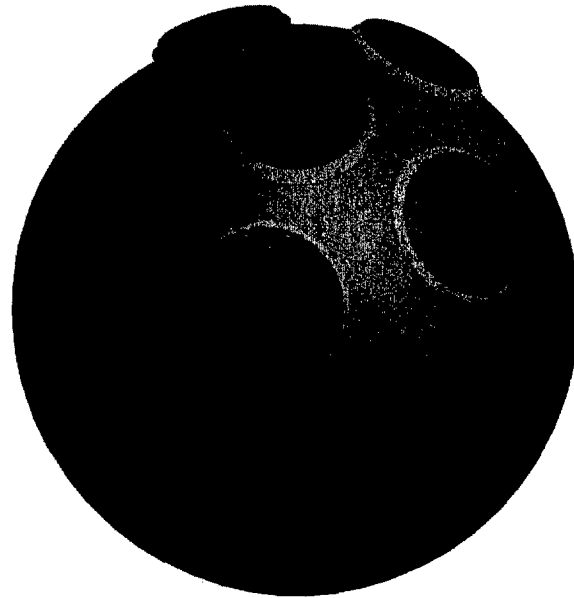
*Figure 4.1.* Spherical array of circular stacked-patch antennas.

coaxial
feed
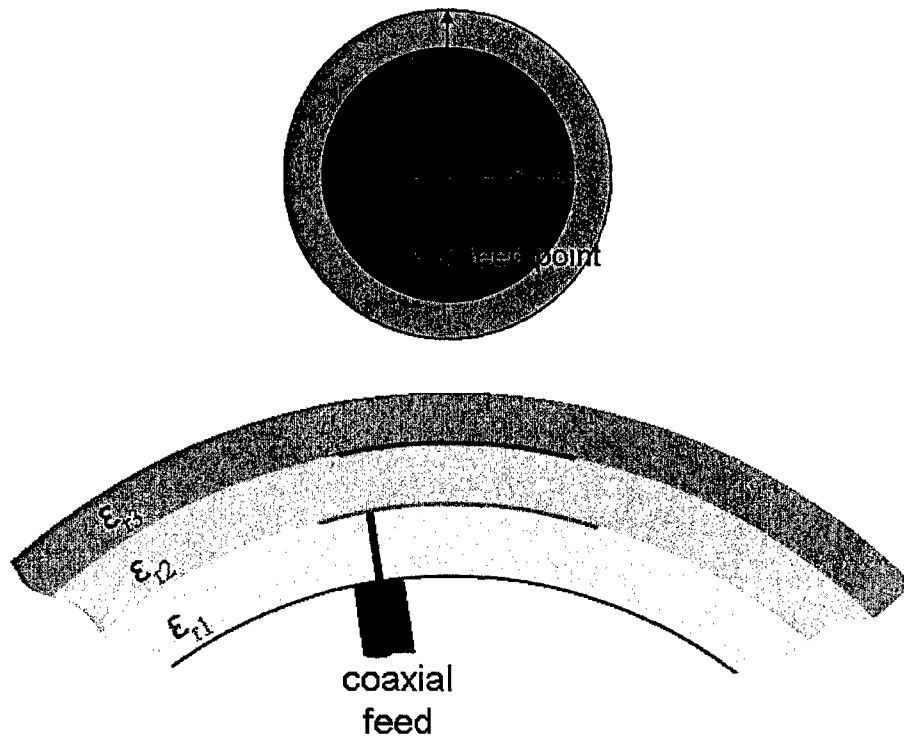
Figure 4.2. The geometry of one circular stacked-patch antenna

$$\tilde{\mathbf{J}}(r,n,m) = \int_{-\pi}^{\pi}\int_{0}^{\pi}\frac{1}{\sqrt{2\pi S(n,m)}}\ \overline{\overline{\mathbf{L}}}(n,m,\theta)\,\mathbf{J}(r,\theta,\phi)\ e^{-jm\phi}\sin\theta\,d\theta\,d\phi \tag{1a}$$

$$\mathbf{J}(r,\theta,\phi) = \sum_{m=-\infty}^{\infty}\sum_{n=|m|}^{\infty}\frac{1}{\sqrt{2\pi S(n,m)}}\ \overline{\overline{\mathbf{L}}}(n,m,\theta)\,\tilde{\mathbf{J}}(r,n,m)e^{jm\phi} \tag{1b}$$

$$\overline{\overline{\mathbf{L}}}(n,m,\theta) = \begin{bmatrix} P_n^{|m|}(\cos\theta)\sqrt{n(n+1)} & 0 & 0 \\[2mm] 0 & \dfrac{\partial P_n^{|m|}(\cos\theta)}{\partial\theta} & \dfrac{-jmP_n^{|m|}(\cos\theta)}{\sin\theta} \\[3mm] 0 & \dfrac{jmP_n^{|m|}(\cos\theta)}{\sin\theta} & \dfrac{\partial P_n^{|m|}(\cos\theta)}{\partial\theta} \end{bmatrix} \tag{1c}$$

$$S(n,m) = \frac{2n(n+1)(n+|m|)!}{(2n+1)(n-|m|)!} \tag{1d}$$

Here $P_n^{|m|}(\cos\theta)$ denotes the associated Legendre function. In [10] the vector-Legendre transformation is defined only for θ and ϕ vector components. We have extended the definition to the r vector component in a symmetric way, i.e. the same coefficient $P_n^{|m|}(\cos\theta)\sqrt{n(n+1)}$ is used in the transformations to the spectral domain and back to the spatial domain [20]. Furthermore, we have modified the definition of the vector-Legendre transformation in order to obtain a numerically stable solution, i.e. it was necessary to insert the term $1/\sqrt{S(n,m)}$ symmetrically into the definition of forward and inverse vector-Legendre transformation [19].

In the case of the coaxial feeding, the radius of the probe is usually a very small fraction of the wavelength and the quantity r_{patch} - r_{GND} is usually small in comparison to the wavelength. Therefore, the probe is modeled as a filament with a constant current

$$\mathbf{J}_{feed}(r,\theta,\phi) = \hat{r}\frac{1}{r^2\sin\theta}\delta(\theta-\theta_{feed})\delta(\phi-\phi_{feed}) \qquad r_{GND}\le r\le r_{patch\_1}, \tag{2}$$

where θ_{feed} and ϕ_{feed} are the θ and ϕ coordinates of the coaxial probe. A radial attachment function is included into the feed model in order to ensure the continuity of the current at the junction between the probe and the patch (a sketch of the attachment mode is given in Fig. 4.3):

$$\mathbf{J}_{att}(r_{patch\_1},\theta',\phi') = \begin{cases} -\dfrac{r_{patch\_1}\sin\theta'}{2\pi R_{att}^2}\hat{e}_{r'} & 0 < r_{patch\_1}\sin\theta' < d_{probe}/2 \\[4mm] -\dfrac{r_{patch\_1}\sin\theta'}{2\pi R_{att}^2}+\dfrac{1}{2\pi r_{patch\_1}\sin\theta'}\hat{e}_{r'} & d_{probe}/2 < r_{patch\_1}\sin\theta' < R_{att} \\[4mm] 0 & r_{patch\_1}\sin\theta' > R_{att} \end{cases} \tag{3}$$

where R_{att} and $d_{probe}/2$ are the radii of the attachment mode and of the probe, respectively. Note that the $\mathbf{J}_{att}$ is given in the local coordinate system in which the probe is placed at the z' axis.

The microstrip line can also be simply modeled as a filament of constant current placed close to the edge of the patch, since microstrip line and coaxial line have similar field distribution around the feeding point. Furthermore, if the feeding point of the coaxial line is close to the patch edge, the input impedances of the patch antennas fed by a microstrip line and fed by a coaxial line are very similar [21] - [23].
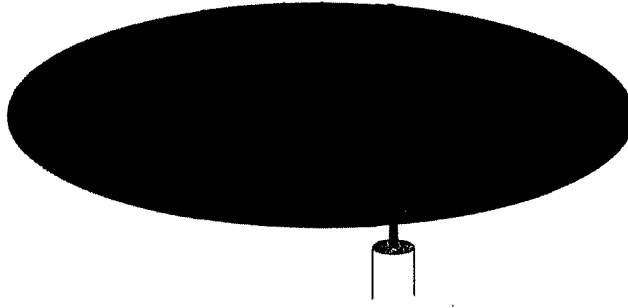
Figure 4.3. Sketch of the attachment mode.

The elements of the MoM matrix [Z] and excitation vector [V] are also calculated in the spectral domain:

$$Z_{ji} = -\sum_{m=-\infty}^{\infty}\sum_{n=|m|}^{\infty} r^2_{patch\_k}\,\widetilde{\mathbf{J}}^T_j(r_{patch\_k},n,-m)\,\overline{\overline{\mathbf{G}}}(n,m,r_{patch\_k}\,|\,r_{patch\_l})\,\widetilde{\mathbf{J}}(r_{patch\_l},n,m) \qquad (4a)$$

$$V_j = \sum_{m=-\infty}^{\infty}\sum_{n=|m|}^{\infty}\frac{1}{\sqrt{2\pi\,S(n,m)}}\hat{r}\cdot\overline{\overline{\mathbf{L}}}(n,m,\theta_{feed})e^{jm\phi_{feed}}\int_{probe}\overline{\overline{\mathbf{G}}}(n,m,r\,|\,r_{patch\_k})\widetilde{\mathbf{J}}_j(r_{patch\_k},n,m)\,dr$$

$$+\int_{\substack{attachment\\function}}\mathbf{J}_{att}(\theta,\phi)\sum_m\sum_{n\geq|m|}\frac{r^2_{patch\_1}}{\sqrt{2\pi S(n,m)}}\overline{\overline{\mathbf{L}}}(n,m,\theta)e^{jm\phi}\,\overline{\overline{\mathbf{G}}}(n,m,r_{patch\_1}\,|\,r_{patch\_k})\widetilde{\mathbf{J}}_j(r_{patch\_k},n,m)\,dS.$$

$$(4b)$$

Notice that basis and test functions can be located at different patches. In the expression for V_j we have used the reaction theorem, $\langle E(J_{probe}),J_{patch}\rangle = \langle E(J_{patch}),J_{probe}\rangle$ [24]. The spectral-domain Green's function $\overline{\overline{\mathbf{G}}}(m,n,r\,|\,r')$ of a general multilayer spherical structure is computed using the G1DMULT algorithm that calculates spectral domain Green's functions of general multilayer planar, circular cylindrical and spherical structures. More details about the G1DMULT algorithm are given in the section 4.1.3 and in the Appendix.

In order to avoid numerical difficulties we have introduced normalized Legendre polynomials

$\overline{P}_n^{|m|}$ and their derivatives as [19] :

$$\overline{P}_n^{|m|} = P_n^{|m|} \sqrt{\frac{(n-|m|)!}{(n+|m|)!}}, \qquad \frac{\partial \overline{P}_n^{|m|}(\cos\theta)}{\partial\theta} = \frac{\partial P_n^{|m|}(\cos\theta)}{\partial\theta} \sqrt{\frac{(n-|m|)!}{(n+|m|)!}}. \qquad (5)$$

Notice that for the normalization factor we have chosen the rapidly growing term inside the term $\sqrt{S(n,m)}$ (see eq. (1.d)). The term $\overline{\overline{L}} / \sqrt{S(n,m)}$ in expressions (1a) and (1b) enables us to calculate normalized Legendre polynomials instead of Legendre polynomials, and $2n(n+1)/(2n+1)$ instead of $S(n,m)$, both of them being numerically stable. Thus, divisions of very large numbers are avoided.

The recursive equations for the normalized Legendre polynomials and their derivatives are:

$$\overline{P}_{n+1}^{|m|}(z)\sqrt{(n+1+|m|)(n+|m|)} = \frac{1}{n-|m|+1} \cdot$$

$$\cdot \left((2n+1)\, z\; \overline{P}_n^{|m|}(z)\sqrt{(n+|m|)(n-|m|+1)} - (n+|m|)\overline{P}_{n-1}^{|m|}(z)\sqrt{(n-|m|)(n-|m|+1)} \right), \qquad (6a)$$

$$(z^2-1)\frac{\partial \overline{P}_n^{|m|}(z)}{\partial z}\sqrt{n+|m|} = nz\overline{P}_n^{|m|}(z)\sqrt{n+|m|} \; - \; (n+|m|)\overline{P}_{n-1}^{|m|}(z)\sqrt{n-|m|}. \qquad (6b)$$

For N_P patches in the array, we need to solve the linear system $[Z][I^k] = [V^k]$ N_P times ($k = 1,...,N_P$), once for each excitation port. In more details, $[V^k]$ vectors correspond to a physical situation in which a unit current is entering the kth port while the remaining N_P - 1 ports are open-circuited. Fortunately, the matrix $[Z]$ is unchanged in all cases. After determining the amplitudes of basis functions $[I^k]$ we calculate the voltage at port l by summing $-\sum V_i^l I_i^k$, i.e., the lk element of the impedance port matrix is $Z_{lk}^{port} = -\sum_i V_i^l I_i^k$. Scattering matrix elements are calculated from the impedance port matrix

$$[S] = ([Z^{port}] - [Z^0])([Z^{port}] + [Z^0])^{-1}, \qquad (7)$$

where $[Z^0]$ is a diagonal matrix with elements Z_0 - the characteristic impedance of the feeding transmission lines.

The far field radiation pattern of a single patch element is obtained as follows. If we consider the θ- and ϕ-component of the electric field in the outermost region with the r-coordinate larger than the r-coordinate of the patch, we have only outward-traveling waves described by the Schelkunoff spherical Hankel function of the second kind $\hat{H}_n^{(2)}(k_0 r)$ [24]. Therefore, in the outermost region we can relate the θ- and ϕ-component of the electric field with different r-coordinates r_1 and r_2 ($r_1 >> r_2$) as

$$\tilde{E}_\theta(r_1,n,m) = \tilde{E}_\theta(r_2,n,m)\; \frac{r_2}{r_1}\frac{\hat{H}_n^{(2)'}(k_0 r_1)}{\hat{H}_n^{(2)'}(k_0 r_2)} \approx \tilde{E}_\theta(r_2,n,m)\; \frac{j^n r_2}{\hat{H}_n^{(2)'}(k_0 r_2)}\frac{e^{-jk_0 r_1}}{r_1} \qquad (8a)$$

$$\tilde{E}_\phi(r_1,n,m) = \tilde{E}_\phi(r_2,n,m) \; \frac{r_2}{r_1} \frac{\hat{H}_n^{(2)}(k_0 r_1)}{\hat{H}_n^{(2)}(k_0 r_2)} \approx \tilde{E}_\phi(r_2,n,m) \; \frac{j^{n+1} r_2}{\hat{H}_n^{(2)}(k_0 r_2)} \frac{e^{-jk_0 r_1}}{r_1} \tag{8b}$$

Here r_1 represents the r-component of the far field pattern. From numerical reasons it is practically to choose the value of r_2 a little bit larger than the radius of the whole antenna structure. The final solution is obtained by superposing all spectral solutions, see eq. (1b). The equations (8a) and (8b) can be easily obtained from equations (22) and (23) of the Appendix.

The radiation pattern of the array is obtained as a superposition of the fields excited by each patch. For that purpose it is convenient to introduce local coordinate systems with the origins located at the center of each patch. The local coordinate system "follows" the patch when it is moved from the central position, i.e. the z' axis of the local system is oriented normal to the patch center. The coordinates in the local coordinate system are determined using the following equations (see [2] for details)

$$\cos\theta' = \sin(\alpha_n)\sin\theta\,\cos(\phi - \beta_n) + \cos(\alpha_n)\cos\theta \tag{9a}$$

$$\cot\phi' = \frac{\cos(\alpha_n)\sin\theta\cos(\phi - \beta_n) - \sin(\alpha_n)\cos\theta}{\sin\theta\sin(\phi - \beta_n)} \tag{9b}$$

where α_n and β_n are the θ- and ϕ-coordinates of the center of each patch in the global coordinate system. The unit vectors in the local coordinate system can be determined from the following equations

$$\hat{e}_{\theta'} = -\frac{\cos\theta\sin\alpha_n\cos(\phi - \beta_{nm}) - \sin\theta\cos\alpha_n}{\sin\theta'}\hat{e}_\theta + \frac{\sin\alpha_n\sin(\phi - \beta_{nm})}{\sin\theta'}\hat{e}_\phi \tag{10a}$$

$$\hat{e}_{\phi'} = -\frac{\sin\alpha_n\sin(\phi - \beta_{nm})}{\sin\theta'}\hat{e}_\theta - \frac{\cos\theta\sin\alpha_n\cos(\phi - \beta_{nm}) - \sin\theta\cos\alpha_n}{\sin\theta'}\hat{e}_\phi \tag{10b}$$

Combining equations (9) and (10) one gets the θ- and ϕ-field components of the field excited by the antenna element with center coordinates (α_n, β_{nm})

$$E_{\theta,\alpha_n\beta_{nm}} = -\left[\frac{\cos\theta\sin\alpha_n\cos(\phi - \beta_{nm}) - \sin\theta\cos\alpha_n}{\sin\theta'} f_\theta(\theta',\phi') + \frac{\sin\alpha_n\sin(\phi - \beta_{nm})}{\sin\theta'} f_\phi(\theta',\phi')\right] \tag{11a}$$

$$E_{\phi,\alpha_n\beta_{nm}} = \left[\frac{\sin\alpha_n\sin(\phi - \beta_{nm})}{\sin\theta'} f_\theta(\theta',\phi') - \frac{\cos\theta\sin\alpha_n\cos(\phi - \beta_{nm}) - \sin\theta\cos\alpha_n}{\sin\theta'} f_\phi(\theta',\phi')\right] \tag{11b}$$

Here f_θ and f_ϕ represent the θ and ϕ components of the far field pattern of the central patch (i.e. of the patch with the center at $\theta = 0$).

4.1.3 Calculation of needed Green's functions

When calculating elements of the MoM matrix one needs to evaluate the Green's function in the spectral domain. Since the basis and test functions are located in different layers, several types of Green's functions are needed. In more details, the following types of Green's functions need to be determined: $\widetilde{\overline{\overline{\mathbf{G}}}}(n,m,r_{patch\_1}|r_{patch\_1})$, $\widetilde{\overline{\overline{\mathbf{G}}}}(n,m,r_{patch\_1}|r_{patch\_2})$, $\widetilde{\overline{\overline{\mathbf{G}}}}(n,m,r_{patch\_2}|r_{patch\_1})$ and $\widetilde{\overline{\overline{\mathbf{G}}}}(n,m,r_{patch\_2}|r_{patch\_2})$. From the reciprocity theorem one can easily derive $\widetilde{\overline{\overline{\mathbf{G}}}}(n,m,r_{patch\_1}|r_{patch\_2}) = \widetilde{\overline{\overline{\mathbf{G}}}}(n,m,r_{patch\_2}|r_{patch\_1})$. Notice that all these Green's functions are for multilayer spherical structures (the structure in example in Figure 4.2 is a three-layer spherical structure).

There are two basic approaches to determine the Green's function of general multilayer structures: either to analytically derive an expression for it and then to code that expression, or to develop a numerical routine for the complete calculation. The analytic approach requires less computer time than the numerical approach. However, it is a very laborious process to analytically determine the Green's functions for substrates with more than two layers. Therefore, in such cases it is convenient to use a numerical algorithm that determines the Green's function directly. Another disadvantage of the analytic approach is that it is valid for a very specific geometry, so that a new derivation of the Green's functions is needed even if the geometry is just slightly different, such as for different locations of the patch antennas inside the multilayer structure. We have developed the G1DMULT algorithm that calculates the spectral-domain Green's functions for planar, circular-cylindrical and spherical multilayer structures, i.e. the algorithm uses advantages of transforming the problem to the spectral domain [20]. The G1DMULT algorithm is described in the Appendix.

The structure of the MoM matrix is influenced by the fact that the antenna element with two patch radiators is considered. For a single stacked-patch antenna the structure of the MoM matrix is given in (12). Notice that each block-matrix is defined according to the domain of the basis and test functions (fed patch or parasitic patch), i.e. for each block-matrix only one type of Green's function needs to be calculated.

$$[Z]=\begin{bmatrix} \begin{bmatrix} Z_{11}^{11} & Z_{12}^{11} & \cdots & Z_{1n}^{11} \\ Z_{21}^{11} & Z_{22}^{11} & \cdots & Z_{2n}^{11} \\ \cdots & \cdots & \cdots & \cdots \\ Z_{n1}^{11} & Z_{n2}^{11} & \cdots & Z_{nn}^{11} \end{bmatrix} & \begin{bmatrix} Z_{11}^{12} & Z_{12}^{12} & \cdots & Z_{1n}^{12} \\ Z_{21}^{12} & Z_{22}^{12} & \cdots & Z_{2n}^{12} \\ \cdots & \cdots & \cdots & \cdots \\ Z_{n1}^{12} & Z_{n2}^{12} & \cdots & Z_{nn}^{12} \end{bmatrix} \\ \begin{bmatrix} Z_{11}^{21} & Z_{12}^{21} & \cdots & Z_{1n}^{21} \\ Z_{21}^{21} & Z_{22}^{21} & \cdots & Z_{2n}^{21} \\ \cdots & \cdots & \cdots & \cdots \\ Z_{n1}^{21} & Z_{n2}^{21} & \cdots & Z_{nn}^{21} \end{bmatrix} & \begin{bmatrix} Z_{11}^{22} & Z_{12}^{22} & \cdots & Z_{1n}^{22} \\ Z_{21}^{22} & Z_{22}^{22} & \cdots & Z_{2n}^{22} \\ \cdots & \cdots & \cdots & \cdots \\ Z_{n1}^{22} & Z_{n2}^{22} & \cdots & Z_{nn}^{22} \end{bmatrix} \end{bmatrix} \tag{12}$$

In eq. (12) the superscript indexes 1 and 2 denote the lower/upper patch where the test and basis functions are located, and the subscript indexes denote the number of the test and basis function.

It is assumed that the current at each patch is approximated with n basis functions. The element Z_{ji}^{kl} can be expressed as (see eq. (3)):

$$Z_{ji}^{kl} = -\sum_{m=-\infty}^{\infty} \sum_{n=|m|}^{\infty} r_{patch\_k}^2 \ \widetilde{\mathbf{J}}_j^T (r_{patch\_k}, n, -m) \ \overline{\overline{\widetilde{\mathbf{G}}}}(n, m, r_{patch\_k} \mid r_{patch\_l}) \widetilde{\mathbf{J}}(r_{patch\_l}, n, m) \quad (13)$$

4.1.4 Vector-Legendre transforms of basis and test functions

As basis functions we have used entire-domain basis functions, i.e. basis functions that are defined on the whole patch. Actual basis functions are determined from the resonant modes of the cylindrical resonator consisting of two parallel PEC circular plates (circular patch and ground plane) and from PMC edge surface. Then, the ith basis function is determined from the relation $\mathbf{J}_i = \hat{n} \times \mathbf{H}_i$. The considered modes are actually the resonant modes of the cavity model of the patch antenna. However, the analysis method is based on the full-wave approach, and therefore the developed program is more accurate and it can analyze more general structures than the program based on the cavity model (stacked-patches, arrays with determined mutual coupling effects).

The basis function, coming from the TM_{kl} mode, is:

(a) irrotational type

$$\mathbf{J}_{kl}(\theta, \phi) = \alpha_{kl} J_k'(\alpha_{kl} \, r_{patch} \, \theta) \cos(k\phi) \hat{\theta} - \frac{k}{r_{patch}\theta} J_k(\alpha_{kl} \, r_{patch} \, \theta) \sin(k\phi) , \quad (14)$$

(b) solenoidal type

$$\mathbf{J}_{kl}(\theta, \phi) = -\frac{k}{r_{patch}\theta} J_k(\beta_{kl} \, r_{patch} \, \theta) \cos(k\phi) \hat{\theta} + \beta_{kl} J_k'(\alpha_{kl} \, r_{patch} \, \theta) \sin(k\phi) , \quad (15)$$

where J_k is the Bessel function of kth order, and α_{kl} and β_{kl} denote constants ($\alpha_{kl} \, r_{patch} \theta_p = \chi'_{kl}$ and $\beta_{kl} \, r_{patch} \theta_p = \chi_{kl}$; χ_{kl} is the lth zero of J_k and χ'_{kl} is the lth zero of J'_k). The vector-Legendre transform of $\mathbf{J}_{kl}$ is

(a) irrotational type

$$\widetilde{J}_\theta(n, m) = \frac{\pi}{\sqrt{2\pi S(n, m)}} \delta(|m| - k) \cdot$$

$$\cdot \left[\int_0^{\theta_p} \overline{P}_n^{|m|}(\cos\theta) \frac{J_k(\alpha_{kl} r_{patch}\theta)}{r_{patch}\theta} d\theta + \int_0^{\theta_p} \frac{d\overline{P}_n^{|m|}}{\partial\theta} \alpha_{kl} \sin\theta \left(J_{k-1}(\alpha_{kl} r_{patch}\theta) - \frac{k J_k(\alpha_{kl} r_{patch}\theta)}{\alpha_{kl} r_{patch}\theta} \right) d\theta \right]$$

$$(16a)$$

$$\tilde{J}_\phi(n,m) = \frac{jm\pi}{\sqrt{2\pi S(n,m)}} \delta(|m|-k) \cdot$$

$$\cdot \left[\int_0^{\theta_p} \overline{P}_n^{|m|}(\cos\theta)\alpha_{kl} \left(J_{k-1}(\alpha_{kl}r_{patch}\theta) - \frac{k J_k(\alpha_{kl}r_{patch}\theta)}{\alpha_{kl}r_{patch}\theta} \right) d\theta + \int_0^{\theta_p} \frac{d\overline{P}_n^{|m|}}{\partial\theta} \frac{J_1(\alpha_{kl}r_{patch}\theta)}{r_{patch}\theta}\sin\theta d\theta \right] \tag{16b}$$

(b) solenoidal type

$$\tilde{J}_\theta(n,m) = \frac{\pi}{\sqrt{2\pi S(n,m)}} \delta(|m|-k) \cdot$$

$$\cdot \left[\int_0^{\theta_p} \frac{d\overline{P}_n^{|m|}}{\partial\theta} \frac{J_k(\beta_{kl}r_{patch}\theta)}{r_{patch}\theta}\sin\theta d\theta + \int_0^{\theta_p} \overline{P}_n^{|m|}(\cos\theta)\beta_{kl} \left(J_{k-1}(\beta_{kl}r_{patch}\theta) - \frac{J_k(\beta_{kl}r_{patch}\theta)}{\beta_{kl}r_{patch}\theta} \right) d\theta \right] \tag{17a}$$

$$\tilde{J}_\phi(n,m) = -\frac{jm\pi}{\sqrt{2\pi S(n,m)}} \delta(|m|-k) \cdot$$

$$\cdot \left[\int_0^{\theta_p} \overline{P}_n^{|m|}(\cos\theta)|m| \frac{J_k(\beta_{kl}r_{patch}\theta)}{r_{patch}\theta} d\theta + \int_0^{\theta_p} \frac{d\overline{P}_n^{|m|}}{\partial\theta} \beta_{kl} \left(J_{k-1}(\beta_{kl}r_{patch}\theta) - \frac{k J_k(\beta_{kl}r_{patch}\theta)}{\beta_{kl}r_{patch}\theta} \right) \sin\theta d\theta \right] \tag{17b}$$

We have made an investigation of the optimal choice of basis and test functions. By comparing the calculated input impedance of the spherical stacked-patch antenna with measured results of equivalent planar antenna we realized that the optimum choice of basis functions includes the following irrotational type basis functions: TM_{11}, TM_{12}, TM_{21} and TM_{31}. The sketch of the used basis functions is given in Fig. 4.4.

When calculating mutual coupling it has been found convenient to introduce a local coordinate system for each patch antenna, similarly as in radiation pattern calculations. The reason for introducing the local coordinate system approach is that it is very cumbersome to analytically express the patch coordinates (and consequently the basis/test functions) if the patch is not located at the pole. The vector-Legendre transform of the basis/test function located at the displaced patch is calculated via using transformation of coordinates from global to local coordinate system. In this way the basis functions in the spectral domain are

$$\tilde{\mathbf{J}}_j(r,n,m) = \iint_{patch} \frac{1}{\sqrt{2\pi\, S(n,m)}} e^{jm\phi}\, \overline{\overline{\mathbf{L}}}(n,m,\theta) \cdot \mathbf{J}_j(r,\theta',\phi')\sin\theta'\, d\theta'\, d\phi' \tag{18}$$

where θ' and ϕ' are coordinates in local coordinate system. Note that both matrix $\mathbf{L}$ and basis functions $\mathbf{J}_i$ are written with respect to the basis $(\hat{e}_\theta, \hat{e}_\phi, \hat{e}_r)$ (basis of the global coordinate system). The connection between local and global coordinate system is given by equations (9) and (10). In eq. (14) we know the coordinates in the local coordinate system, and we need to determine the coordinates in the global coordinate system. In other words, we need to determine the inverse transformation of the coordinate system:

TM$_{11}$ mode

TM$_{12}$ mode

TM$_{21}$ mode

TM$_{31}$ mode
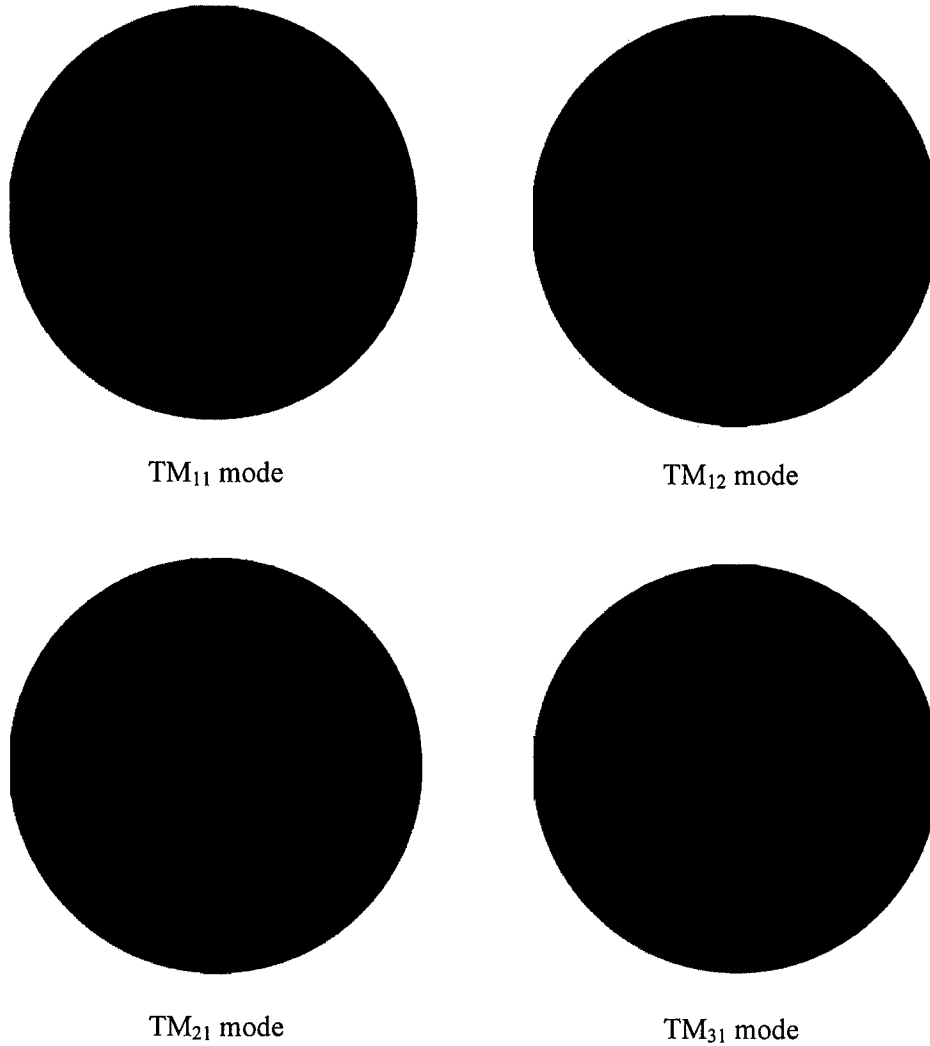
Figure 4.4. Sketch of the applied basis and test functions.

$$\cos\theta = -\sin\alpha_n \sin\theta'\cos\phi + \cos\alpha_n \cos\theta' \qquad (19a)$$

$$\cot\phi = \frac{\cos\alpha_n \sin\theta'\cos\phi' + \sin\alpha_n \cos\theta'}{\sin\theta'\sin\phi'} \qquad (19b)$$

Equation (19) is obtained in 3 steps: the local coordinate system is first rotated an angle of π, then it is tilted an angle of α_n, and finally it is rotated an angle of π-β_n. The unit vectors in the global coordinate system can be determined by rotating the unit vectors of the local coordinate system by an - angle $-\psi$ (inverse rotation). Since eq. (10) can be actually written as

$$\hat{e}_{\theta'} = \cos\psi \, \hat{e}_{\theta} + \sin\psi \, \hat{e}_{\phi} \tag{20a}$$

$$\hat{e}_{\phi'} = -\sin\psi \, \hat{e}_{\theta} + \cos\psi \, \hat{e}_{\phi}, \tag{20b}$$

the inverse transformation can be easily determined by replacing ψ with $-\psi$:

$$\hat{e}_{\theta} = -\frac{\cos\theta\sin\alpha_n\cos(\phi-\beta_{nm})-\sin\theta\cos\alpha_n}{\sin\theta'}\hat{e}_{\theta'} - \frac{\sin\alpha_n\sin(\phi-\beta_{nm})}{\sin\theta'}\hat{e}_{\phi'} \tag{21a}$$

$$\hat{e}_{\phi} = \frac{\sin\alpha_n\sin(\phi-\beta_{nm})}{\sin\theta'}\hat{e}_{\theta'} - \frac{\cos\theta\sin\alpha_n\cos(\phi-\beta_{nm})-\sin\theta\cos\alpha_n}{\sin\theta'}\hat{e}_{\phi'} \tag{21b}$$

Notice that there is a simple relation between vector-Legendre transforms of basis /test functions defined at different patches with the same θ coordinate: $\tilde{\mathbf{J}}_{j1}(n,m) = \tilde{\mathbf{J}}_{j2}(n,m)e^{jm(\beta_1-\beta_2)}$, where β_1 and β_2 denote the ϕ coordinate of the patch centers. In other words, when considering a set of patches with the same θ coordinate, one needs to calculate the vector-Legendre transforms of basis /test functions for one patch only.

4.1.5 Structure of the program

If one considers the expressions needed to be calculated when implementing the spectral-domain moment method (equations (3) and (4)), one can notice that several parts depend only on geometry, i.e. they do not depend on frequency. For example, the vector-Legendre transforms of basis and test functions depend only on angular dimensions. Furthermore, if one considers the expressions that are used inside the G1DMULT algorithm (see Appendix), it can be seen that all expressions depend only on the spectral variable n, i.e. they do not depend on the spectral variable m (the φ dependence is included in the matrix $\overline{\overline{L}}$, see eqs. (1a)-(1d)). Therefore, the needed computer time can be drastically reduced if one precalculates parts that do not depend on frequency. More precisely, the vector-Legendre transforms of basis and test functions and the needed Legendre functions are calculated only once at the beginning of the program, whereas the spectral-domain Green's functions are calculated only once per each frequency point outside the loop over m. The flow chart of the developed program is given in Figure 4.5.
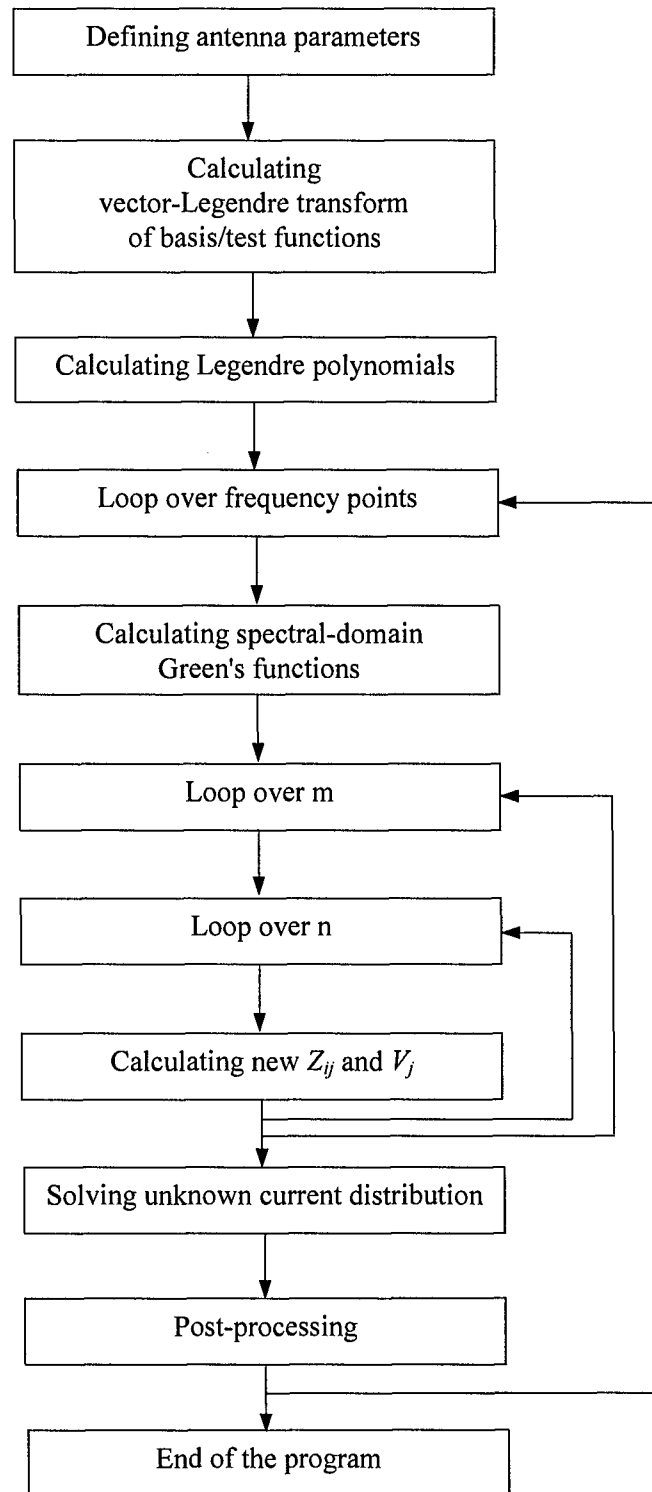
*Figure 4.5.* The flow chart of the program SMiSPA.
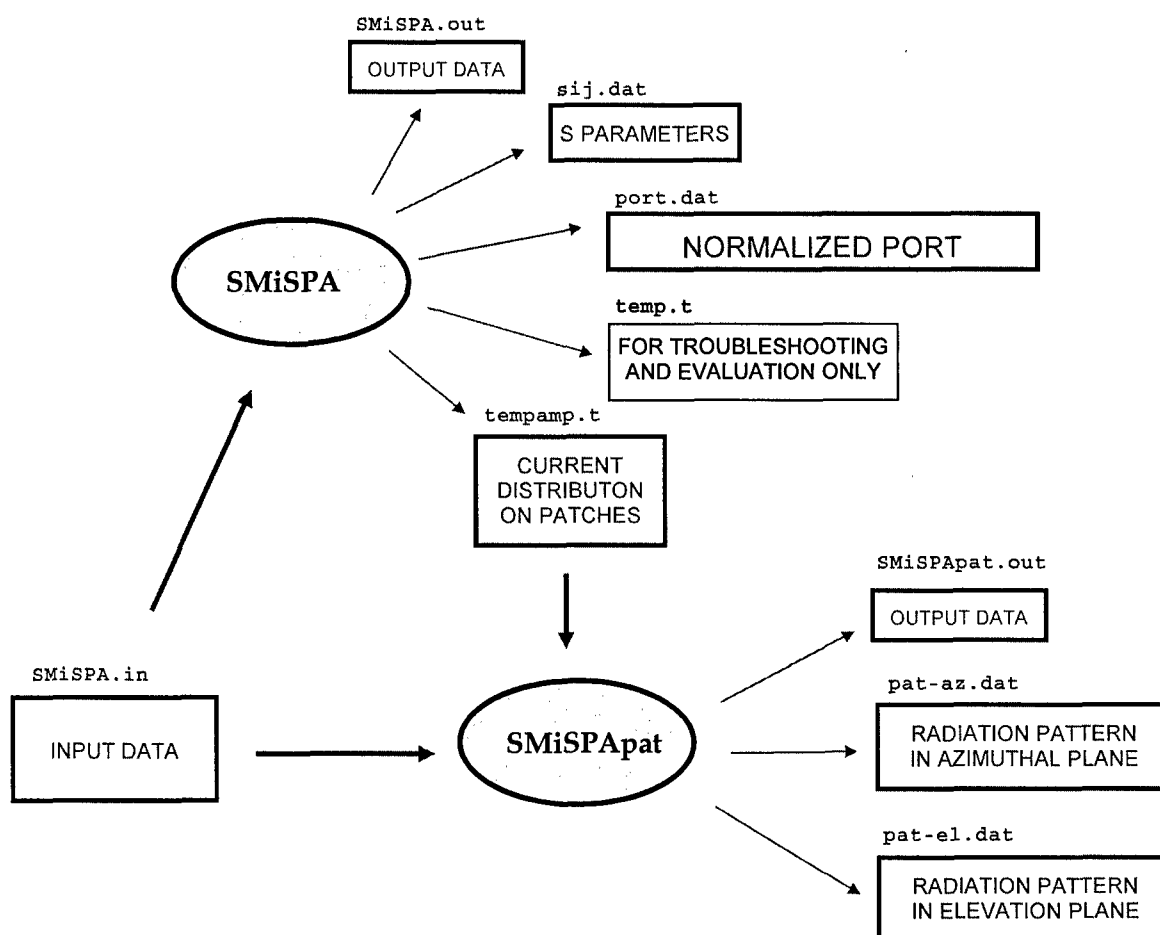
Figure 4.6. Input and output files for the programs SMiSPA and SMiSPApat.

We have named the developed program SMiSPA -- program for analyzing Spherical Microstrip Stacked-Patch Arrays. Since the requirements on the calculation of the radiation pattern are quite different from the requirements on calculation of the current distribution, we have divided the developed program into two programs: SMiSPA and SMiSPApat. By means of the SMiSPA program the current distribution at each patch in the array can be calculated, as well as input impedance at each input port and mutual coupling between each two patches. The SMiSPApat program then calculates the radiation pattern of the array, with or without taking mutual coupling into account. The SMiSPA and SMiSPApat programs communicate via input/output files, and Figure 4.6 shows the structure of all input and output files.

The program SMiSPA/SMiSPApat can calculate the following antenna characteristics:

(a) current distribution at each patch in the array

(b) input impedance of each patch in the array

(c) mutual coupling between each two patches in the array

(d) radiation pattern of the array when all mutual couplings are taken into account

4.1.6 Appendix

G1DMULT algorithm. Planar, circular cylindrical and spherical multilayer structures have one property in common: the structure is homogeneous in two dimensions, and varies in the third dimension. For example, the spherical structure varies in the radial direction and is homogeneous in θ and ϕ directions. Therefore, we can call such structures one-dimensional structures since they vary only in one dimension. The problem of determining the E- and H-fields radiated by a source embedded in a one-dimensional structure can be simplified if we perform the two-dimensional Fourier transformation in the coordinates in which the structure is homogeneous. In the spherical case we perform the vector-Legendre transformation (eqs. (1a)-(1d)), and in the cylindrical case we perform the Fourier transformation in axial direction and the Fourier series in ϕ direction. For each spectral component of the source the excited electromagnetic field in two directions for which the structure is homogeneous has the same harmonic variation as the source. As a result, only the electromagnetic field variation in the normal direction is unknown. In other words, our original three-dimensional problem is transformed into a spectrum of one-dimensional problems, which is much easier to solve.

The G1DMULT algorithm is based on dividing the multilayer problem into equivalent subproblems, one for each dielectric layer. In the spherical case the fields inside each layer are in the form (e.g. E_ϕ component)

$$\widetilde{E}_\phi(r,n,m) = a^i_{nm}\hat{H}^{(2)}_n(k_i r) + b^i_{nm}\hat{J}_n(k_i r) \tag{22}$$

Here $\hat{H}^{(2)}_n$ and $\hat{J}_n$ are the Schelkunoff spherical Bessel and Hankel functions [24], k_i is the wave number in i-th layer, and a^i_{nm} and b^i_{nm} are the unknown coefficients to be determined. The equivalent subproblems are related (and the coefficients a^i_{nm} and b^i_{nm} are calculated) by forcing the continuity of tangential components of electric and magnetic fields.

By means of the vector-Legendre transformation, the three-dimensional excitation currents are transformed into harmonic current shells (current sheets in the planar case and current tubes in the cylindrical case). The core problem inside the G1DMULT algorithm is to calculate the electromagnetic field in the homogeneous space radiated by an electric and a magnetic harmonic current shell of radius r_s

a) from $\widetilde{J}_\theta(r_s,n,m)$

$$\widetilde{E}_\theta(r,n,m) = -\frac{\eta r_s}{r}\widetilde{J}_\theta(r_s,n,m)\cdot\begin{cases}\hat{H}^{(2)}_n{}'(kr_s)\hat{J}_n{}'(kr) & r<r_s \\ \hat{J}_n{}'(kr_s)\hat{H}^{(2)}_n{}'(kr) & r\geq r_s\end{cases} \tag{23a}$$

$$\widetilde{E}_r(r,n,m) = -\frac{\eta r_s}{kr^2}\sqrt{n(n+1)}\;\widetilde{J}_\theta(r_s,n,m)\cdot\begin{cases}\hat{H}^{(2)}_n{}'(kr_s)\hat{J}_n(kr) & r<r_s \\ \hat{J}_n{}'(kr_s)\hat{H}^{(2)}_n(kr) & r\geq r_s\end{cases} \tag{23b}$$

$$\widetilde{H}_\phi(r,n,m) = \frac{jr_s}{r}\widetilde{J}_\theta(r_s,n,m)\cdot\begin{cases}\hat{H}^{(2)}_n{}'(kr_s)\hat{J}_n(kr) & r<r_s \\ \hat{J}_n{}'(kr_s)\hat{H}^{(2)}_n(kr) & r\geq r_s\end{cases} \tag{23c}$$

b) from $\widetilde{J}_\phi(r_s,n,m)$

$$\widetilde{E}_\phi(r,n,m) = -\frac{\eta r_s}{r}\, \widetilde{J}_\phi(r_s,n,m) \cdot \begin{cases} \hat{H}_n^{(2)}(kr_s)\hat{J}_n(kr) & r < r_s \\ \hat{J}_n(kr_s)\hat{H}_n^{(2)}(kr) & r \geq r_s \end{cases} \tag{23d}$$

$$\widetilde{H}_\theta(r,n,m) = \frac{jr_s}{r}\, \widetilde{J}_\phi(r_s,n,m) \cdot \begin{cases} \hat{H}_n^{(2)}(kr_s)\hat{J}_n{}'(kr) & r < r_s \\ \hat{J}_n(kr_s)\hat{H}_n^{(2)\,'}(kr) & r \geq r_s \end{cases} \tag{23e}$$

$$\widetilde{H}_r(r,n,m) = \frac{jr_s}{kr^2}\sqrt{n(n+1)}\;\widetilde{J}_\phi(r_s,n,m) \cdot \begin{cases} \hat{H}_n^{(2)}(kr_s)\hat{J}_n(kr) & r < r_s \\ \hat{J}_n(kr_s)\hat{H}_n^{(2)}(kr) & r \geq r_s \end{cases} \tag{23f}$$

For planar and cylindrical cases the core problem is to determine the electromagnetic field in the homogeneous space radiated by an electric and a magnetic harmonic current sheet and tube, respectively. Fields excited by the magnetic current shell can be easily determined by the duality concept [24]. Fields caused by the r-directed sources are evaluated using the transverse replacement current $\mathbf{M}^{rep} = (j\eta/k)\,\nabla \times J_r\hat{r}$ [24].

Numerical problems can occur when calculating Bessel/Hankel functions of large order (they are needed if the considered spherical structure has a large radius in terms of the wavelength). In order to obtain a numerically stable program we have implemented Debye's asymptotic formulas for Bessel and Hankel functions of large orders [25], [26]

$$J_{m+1/2}(\zeta) \cong \sqrt{\frac{\pi\zeta}{2}}\,\frac{e^{(m+1/2)(\tanh\alpha - \alpha)}}{\sqrt{2\pi(m+1/2)\tanh\alpha}}\left[1 + \frac{3t - 5t^3}{24(m+1/2)}\right] \tag{24a}$$

$$H^{(2)}_{m+1/2}(\zeta) \cong j\sqrt{\frac{\pi\zeta}{2}}\,\frac{e^{(m+1/2)(\alpha - \tanh\alpha)}}{\sqrt{0.5\pi(m+1/2)\tanh\alpha}}\left[1 - \frac{3t - 5t^3}{24(m+1/2)}\right]. \tag{24b}$$

Here α and t are defined as $\cosh\alpha = (m+1/2)/\zeta$ and $t = \coth\alpha$. Notice that the exponential parts of Bessel and Hankel approximate formulas have opposite behavior, i.e. the arguments of the exponential functions have the same absolute values and opposite signs. On the other hand the Green's functions of spherical multilayer structures can be written in terms of the product $\hat{J}_{m+1/2}(\,\cdot\,)\;\hat{H}^{(2)}_{m+1/2}(\,\cdot\,)$ (see Appendix for exact expressions). Therefore, Debye's asymptotic formulas are applied to the product $\hat{J}_{m+1/2}(\,\cdot\,)\;\hat{H}^{(2)}_{m+1/2}(\,\cdot\,)$ with extracted exponential parts, i.e. the exponential part is calculated for the product $\hat{J}_{m+1/2}(\,\cdot\,)\;\hat{H}^{(2)}_{m+1/2}(\,\cdot\,)$. Thereby, we avoid numerical problems since the individual exponential factors are suppressed. The asymptotic formulas are used if the order of Bessel/Hankel function is larger than $5k_0r_{patch}$ or if it is larger than 250. For $|m+1/2 - \zeta|^{1/3} \leq O(m)$ Debye's formulas are not accurate, and for all m in that range the Olver's asymptotic formulas are used [25], [27].

4.2 Effects of the Sphere Curvature

The effects of the sphere size on the input impedance, mutual coupling and radiation pattern will be illustrated in the following examples. We consider the circular stack-patch antenna that is embedded in a three-layer spherical structure (see Fig. 4.2). The permittivity and thickness of each layer are ε_{r1}=2.45, h_1 = 1.52 mm, ε_{r2} = 1.22, h_2 = 6.352 mm and ε_{r3} = 2.45, h_3 = 0.761 mm, respectively. The diameters of the lower and upper patches are 2.647 cm and 2.673 cm, respectively. The lower patch is excited with a coaxial transmission line, and the excitation position is 0.794 cm relative to patch center.

The influence of the sphere radius on input impedance of spherical single patch and stacked-patch antennas is shown in Figures 4.7 - 4.9. For comparison, the measured input impedance of the planar stacked-patch antenna with same dimensions is also given in Fig. 4.9. It can be seen that the sphere radius mostly influences the resonant frequency, i.e. the shape and the magnitude of the impedance curve is almost the same for all chosen radii of the structure (0.5 λ – 5.0 λ at 4.0 GHz). Therefore, it is almost impossible to distinguish impedance curves in the Smith chart. Notice that the shape of impedance locus of a stacked-patch antenna can be interpreted as a superposition of two impedance loci of single patch antennas, i.e. each patch of the stacked-patch antenna can be treated as a separate resonator.

The effect of the radius of the ground plane (grounded shell) on radiation pattern is given in Fig. 4.10. For comparison, the calculated radiation pattern of the planar patch antenna with same dimensions is also given. The operating frequency is 4.5 GHz. It can be seen that with enlarging the radius of the sphere the main lobe of the spherical patch antenna approaches the main lobe of the planar counterpart, i.e. the main lobe is wider for spherical patch antennas, especially in H-plane. As expected, the back-radiation is smaller for spheres with larger radius.

The comparison of mutual coupling levels of a two-patch array of single patch and stacked-patch antennas is given in Fig. 4.11. The distance between patch centers is 12 cm (1.6 λ at 4.0 GHz). In order to match the single patch antenna, the position of the feed point is placed 0.4 cm relative to the patch center; other antenna dimensions are the same as before. Notice that from the shape of the magnitude of S_{21} parameter it can be seen that the stacked-patches have wider bandwidth (which was the main motivation for their development). It is interesting to see that the coupling level in both E- and H-planes is higher for single patch antennas than for the stacked-patch antennas in the frequency band where the single patch antenna is matched. This result is not intuitive since one would expect that the stacked-patch antennas have higher coupling since the coupling results from interaction of 4 patches comparing to the single patch configuration where the coupling results from interaction of 2 patches.

The influence of the sphere radius on mutual coupling level is shown in Fig. 4.12 where the magnitude of the S_{21} parameter, both in E- and H-plane, is shown as a function of spacing between patch edges. Two single circular patches of a diameter 1.86 cm are printed on a

grounded dielectric layer (ε_r = 2.5, h_l = 0.16 cm). The position of the feed point is 0.2 cm relative to the patch center. The coupling level is compared to the measured results of equivalent planar case [30]. It can be seen that the coupling is weaker for spherical case in comparison to the planar one. For smaller structure radii mutual coupling starts to be oscillatory due to interference of forward and backward propagating waves around the sphere.
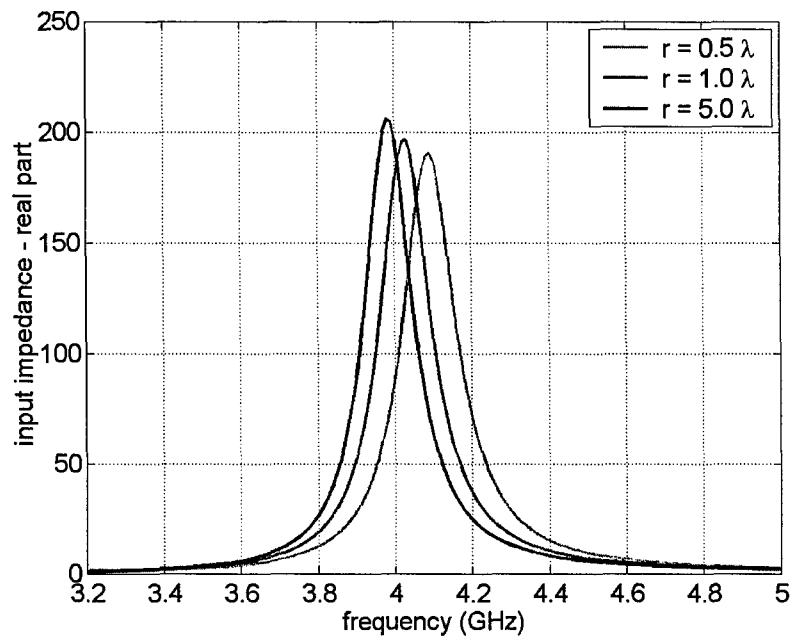

(a)
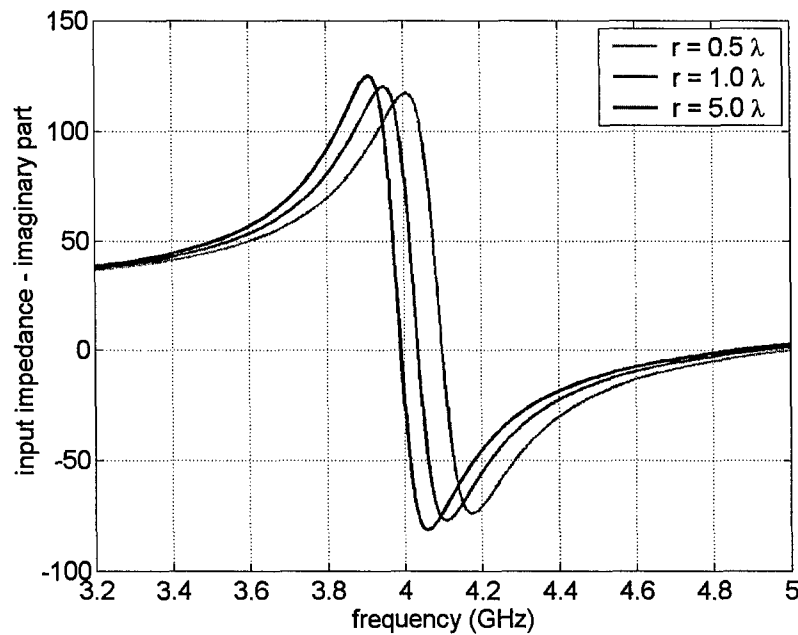
(b)

Figure 4.7. Input impedance of a single patch antenna for different sphere radii; (a) real part, (b) imaginary part.
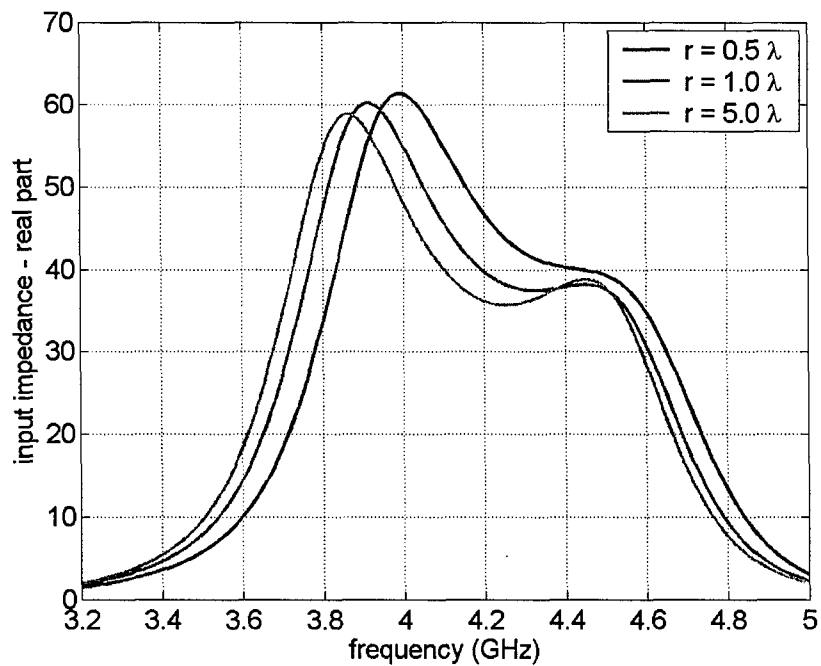
(a)
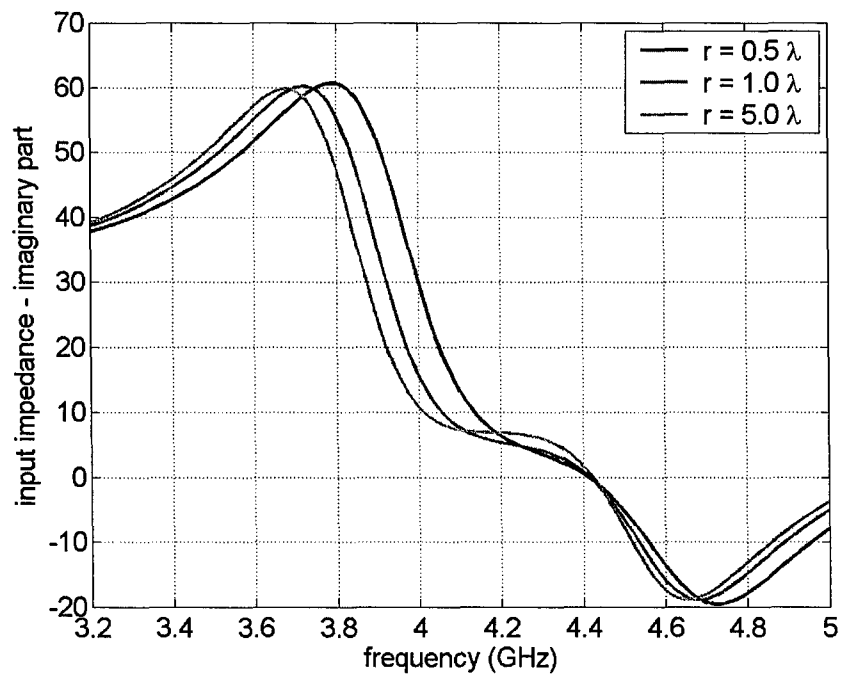
(b)

Figure 4.8. Input impedance of a stacked-patch antenna for different sphere radii; (a) real part, (b) imaginary part.
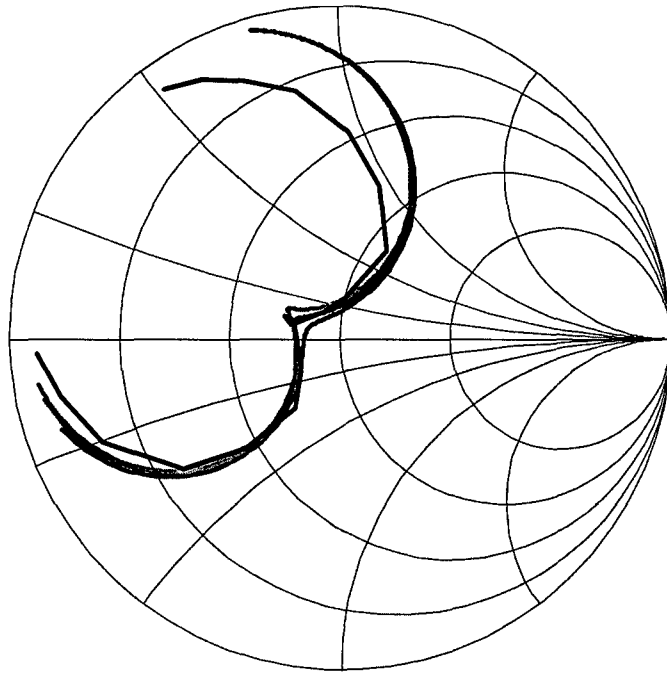
Figure 4.9. Input impedance of a stacked-patch antenna for different sphere radii; (a) real part, (b) imaginary part. ——— $R_{GND} = 0.5\ \lambda$, ——— $R_{GND} = 0.5\ \lambda$, ——— $R_{GND} = 5.0\ \lambda$, ——— measured (planar).
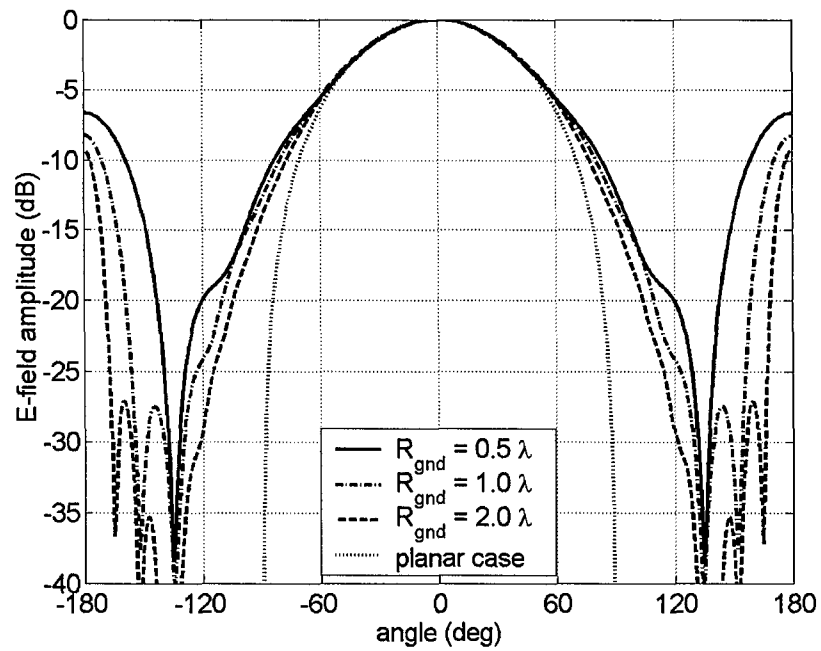
(a)
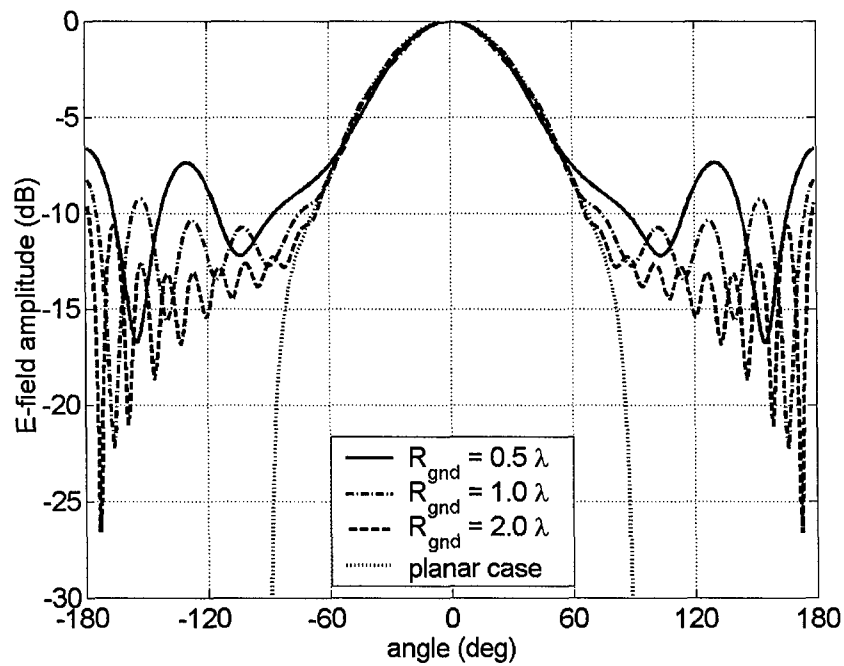
(b)

Figure 4.10. Radiation pattern of a spherical stacked-patch antenna for different sphere radii; (a) H-plane, (b) E-plane.
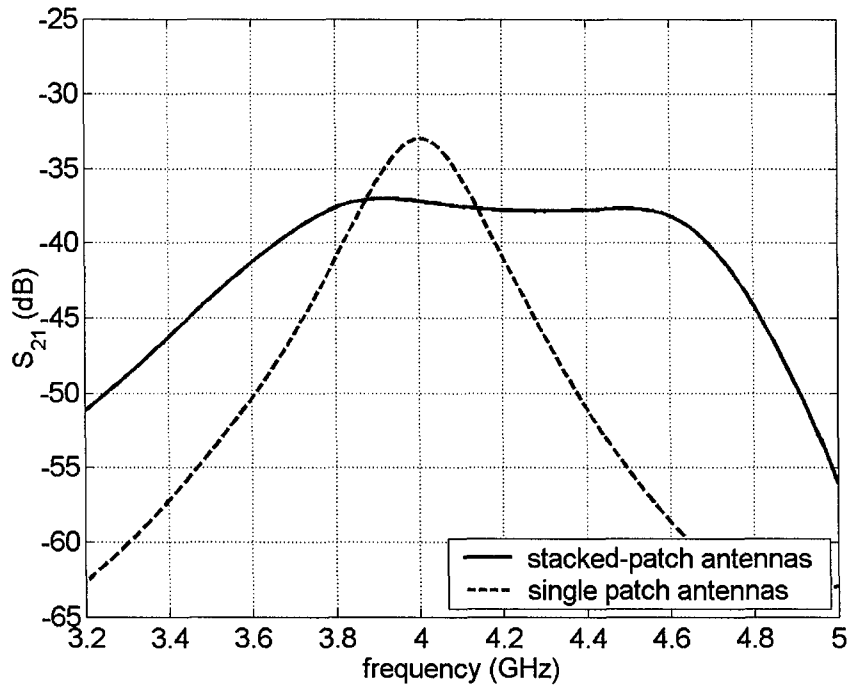
(a)
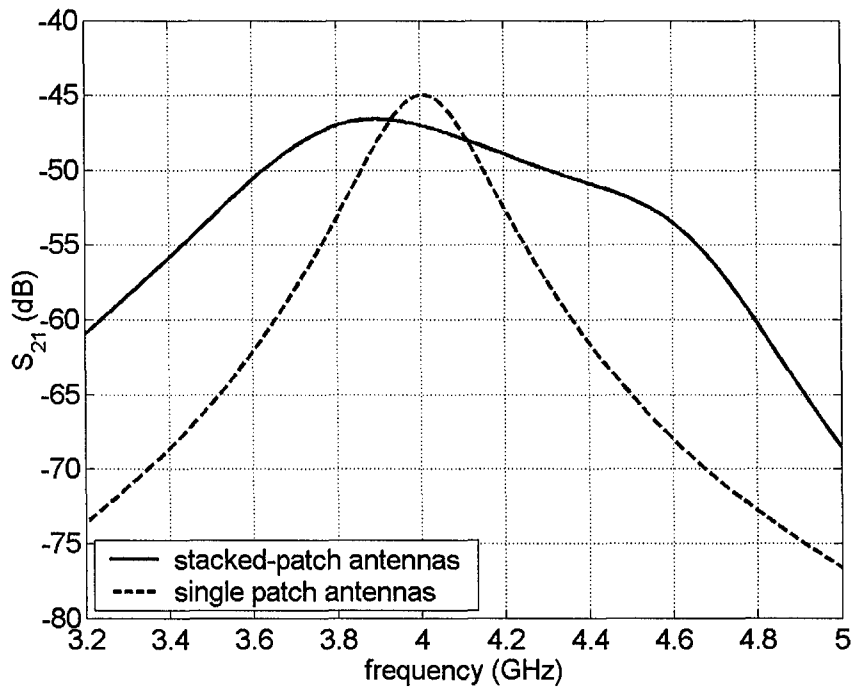
(b)

Figure 4.11. Calculated magnitude of S_{21} parameter of a two-patch array as a function of frequency; (a) coupling in E-plane, (b) coupling in H-plane.
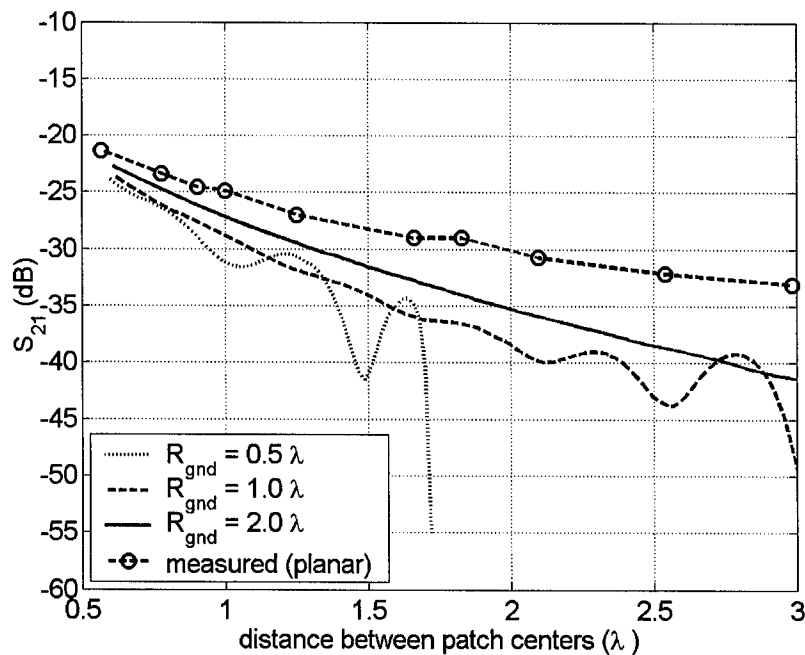
(a)
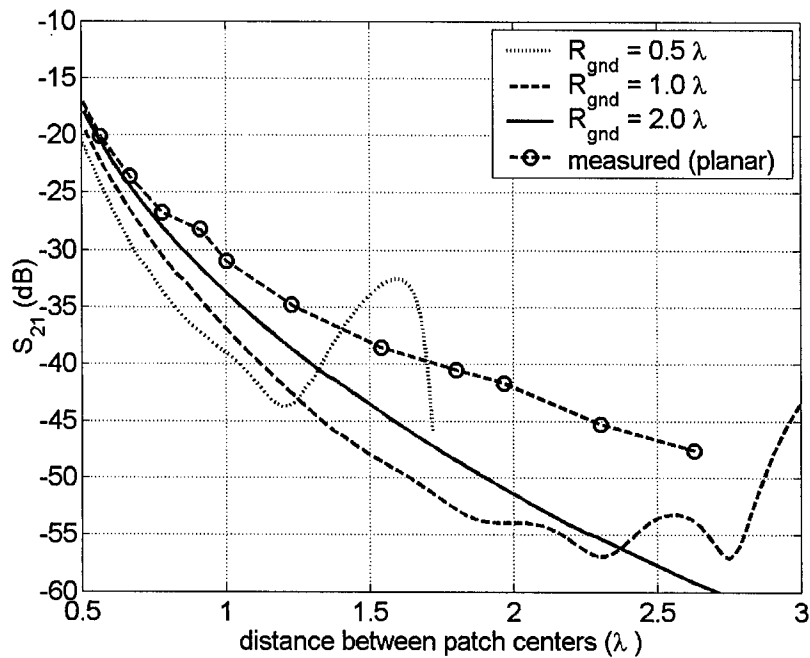
(b)

Figure 4.12. Calculated magnitude of S_{21} parameter of a two-patch array as a function of spacing between patch centers; (a) *E*-plane coupling, (b) *H*-plane coupling.

4.3 Laboratory model

In order to validate the program a laboratory model was developed where it is simple to measure different array configurations (Fig. 4.13). The model was built from a copper sphere of radius $a =$ 18.5 cm on which patches were mounted at different positions. Mounting of patches at arbitrary positions is very simple: one just needs to place an SMA connector at the desired position on the grounded shell. Small styrofoam cubes ($\varepsilon_r \approx 1.0$) are used as spacers between patches and the grounded shell. Note that the patches are made from a sphere of appropriate radius since it is important that patches follow the spherical structure (see discussion below).

The comparison of calculated and measured input impedance and mutual coupling is given in the following examples. Experimental spherical patch and stacked-patch antennas of two different sizes were built (their dimensions are given in the following tables). The goal was to test the program for different angular dimensions of the patch, i.e. the diameter of the larger patch is 36.7 deg, whereas the diameter of the smaller patch 18.7 deg. In the realization of the spherical patch antennas we noticed a problem with deviation from the spherical symmetry, i.e. we have made the upper patches from copper sphere with smaller radius of curvature than required. Consequently, the measured resonant frequency was too low for all stacked-patch configurations (see the discussion about sensitivity on deviation from spherical symmetry in the next section). In future, we plan to make a new experimental model of spherical stacked-patch arrays where all patches will have appropriate curvatures.

In this section we will present the following experimental results:

1. Single–layer patch antenna of diameter 12.2 cm (36.7 deg)
2. Stacked patch antenna of diameter 12.2 cm (36.7 deg)
3. Single–layer patch antenna of diameter 6.2 cm (18.7 deg)
4. Stacked patch antenna of diameter 6.2 cm (18.7 deg)
5. Array of two stacked-patch antennas of diameter 6.2 cm (18.7 deg)

In all considered cases the measured results are compared with the calculated results.

coaxially fed
stacked-patch

copper half-sphere
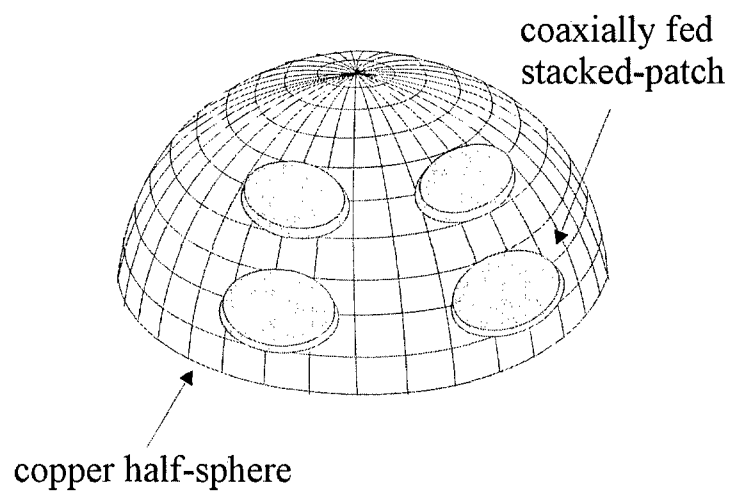
(a)

(b)

Figure 4.13. Sketch (a) and photo (b) of the developed laboratory model.

4.3.1 Spherical single-layer patch antenna of diameter 12.2 cm

Antenna description

Type: Circular stacked-patch antenna mounted on spherical structure

Frequency: 1.0 GHz – 1.8 GHz

The mechanical data of the stacked-patch antenna is given in the following table:

no.of layer	layer description	relative permittivity	Loss tangent	inner radius	outer radius	Thickness
-	ground sphere	-	-	18.5 cm	18.5 cm	-
1	Dielactric layer (air)	1.0	0.0	18.5 cm	19.05 cm	0.55 cm

Circular stacked-patch element data:

Patch number	Element is printed on	Diameter
1	Outer shell of layer no. 1	12.2 cm

Coaxial excitation position, relative to patch center: **5.15 cm.**

Array configuration: **single-layer patch element.**
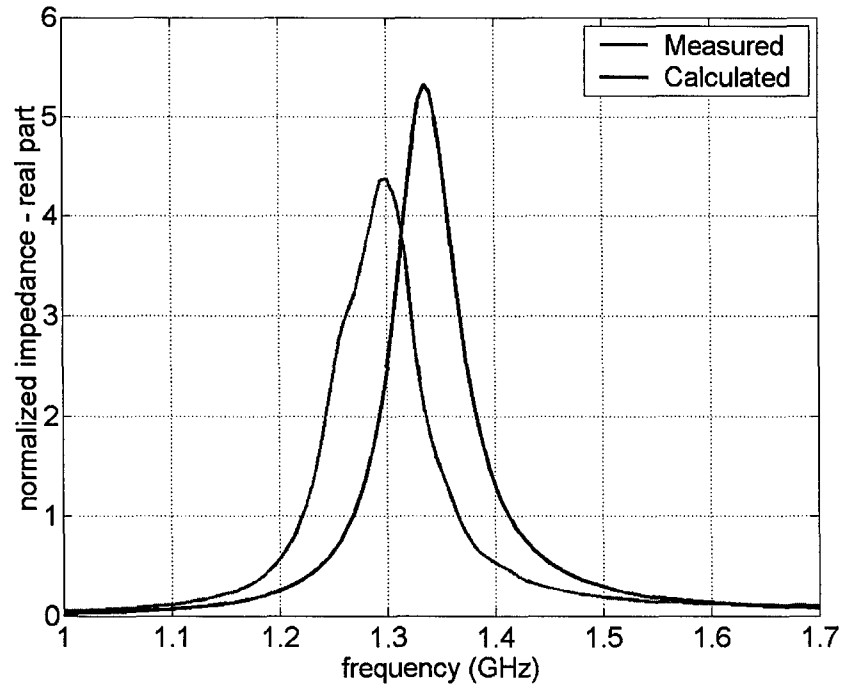
(a)
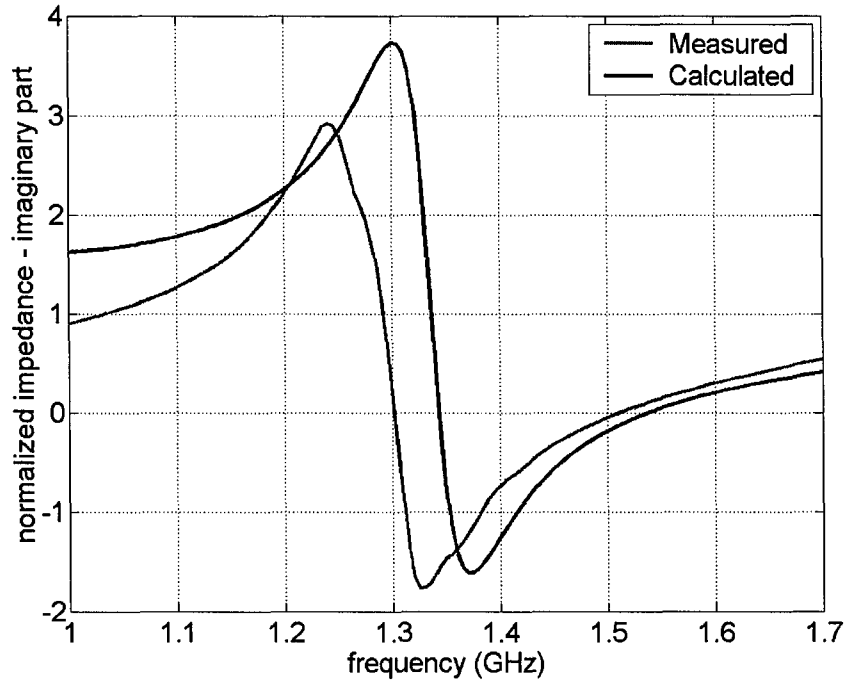
(b)

Figure 4.14. The comparison of calculated and measured input impedance.
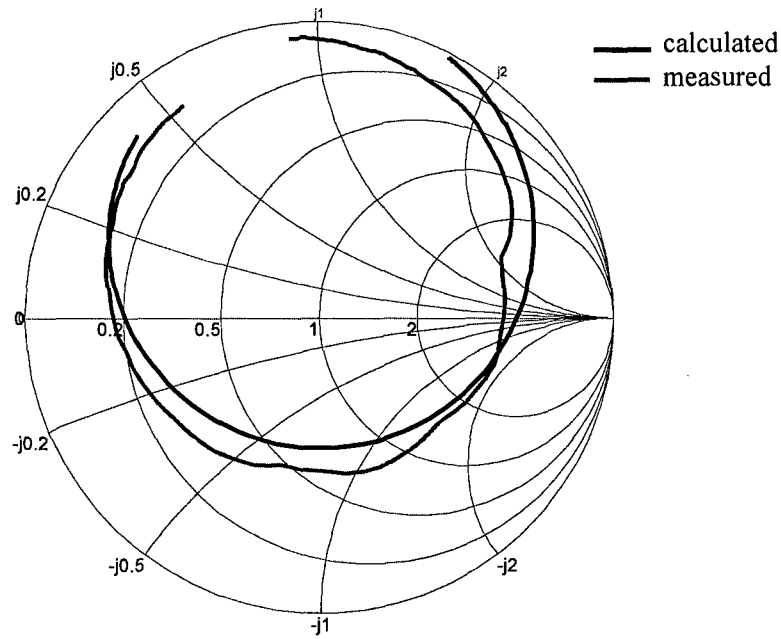
Figure 4.15. The comparison of calculated and measured input impedance.

Unfortunately, in this case we did not manage to develop a stacked-patch antenna that perfectly follows the spherical symmetry. As it can be seen from the shape of the measured input impedance locus in Fig. 4.15, the orthogonal current mode (i.e. the mode that is rotated for 90 degrees) is also excited. The large sensitivity on deviation from the spherical symmetry is discussed in details in section 4.3.

4.3.2 Spherical stacked-patch antenna of diameter 12.2 cm

Antenna description

Type: Circular stacked-patch antenna mounted on spherical structure

Frequency: 1.0 GHz – 1.8 GHz

The mechanical data of the stacked-patch antenna is given in the following table:

no.of layer	layer description	relative permittivity	Loss tangent	inner radius	outer radius	Thickness
-	ground sphere	-	-	18.5 cm	18.5 cm	-
1	Dielactric layer (air)	1.0	0.0	18.5 cm	19.05 cm	0.55 cm
2	Dielactric layer (air)	1.0	0.0	19.05 cm	19.6 cm	0.55 cm

Circular stacked-patch element data:

Patch number	Element is printed on	Diameter
1	Outer shell of layer no. 1	12.2 cm
2	Outer shell of layer no. 2	10.8 cm

Coaxial excitation position, relative to patch center: **5.15 cm.**

Array configuration: **single stacked-patch element.**
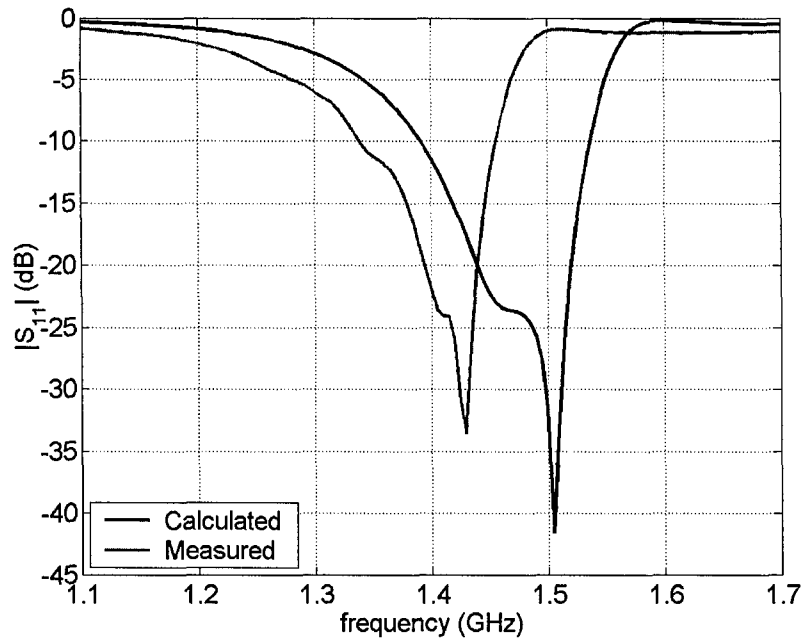
Figure 4.16. The comparison of calculated and measured return loss.
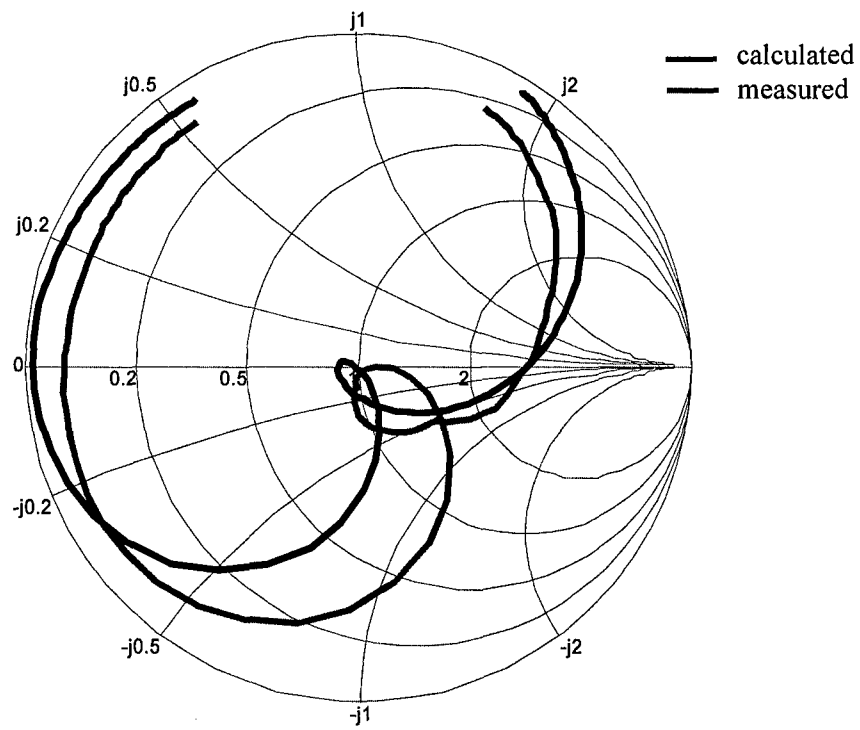
Figure 4.17. The comparison of calculated and measured input impedance.

4.3.3 Spherical single-layer patch antenna of diameter 6.2 cm

Antenna description

Type: Circular patch antenna mounted on spherical structure

Frequency: 2.0 GHz – 3.0 GHz

The mechanical and dielectric data of the single-layer patch antenna is given in the following tables:

No.of layer	Layer description	Relative permittivity	Loss tangent	Inner radius	Outer radius	Thickness
-	ground sphere	-	-	18.5 cm	18.5 cm	-
1	Dielactric layer (air)	1.0	0.0	18.5 cm	19.02 cm	0.52 cm

Circular patch element data:

Patch number	Element is printed on	Diameter
1	Outer shell of layer no. 1	6.2 cm

Coaxial excitation position, relative to patch center: **2.0 cm**

Array configuration: **single-layer patch element.**

(a)

(b)
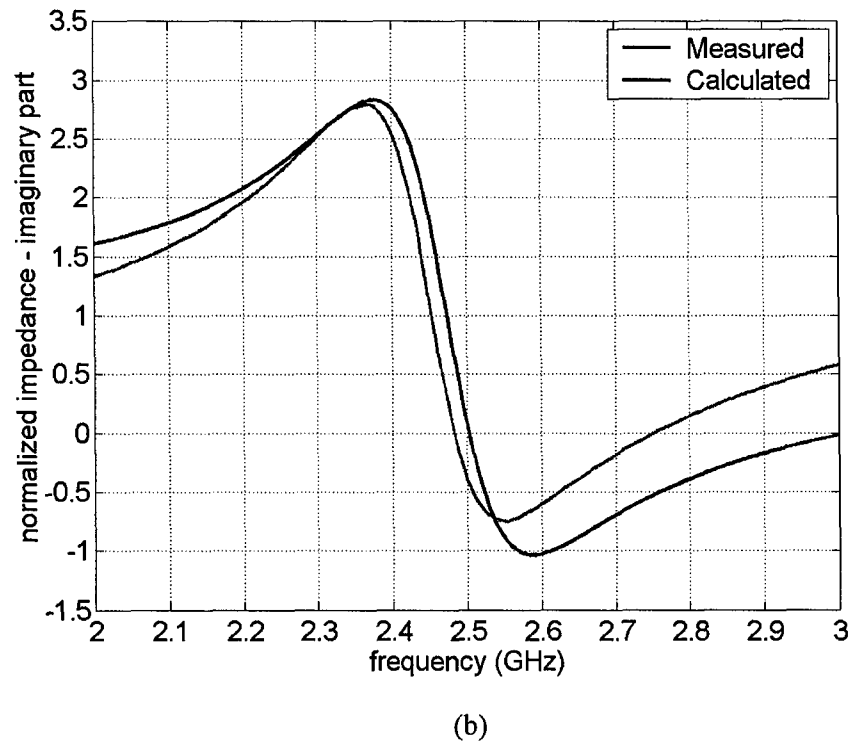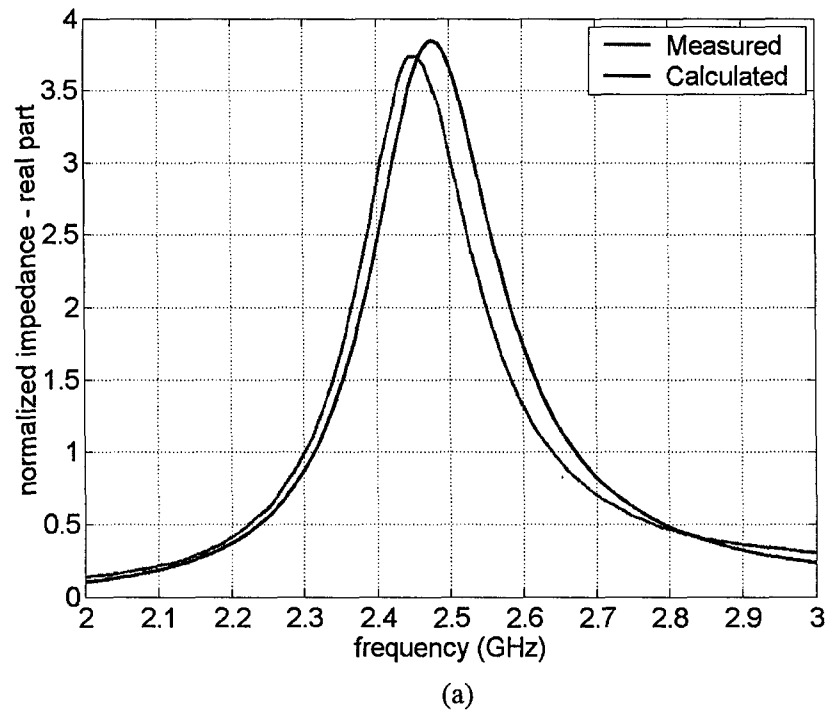
*Figure 4.18.* The comparison of calculated and measured input impedance.

4.3.4 Spherical stacked-patch antenna of diameter 6.2 cm

<u>Antenna description</u>

Type: Circular stacked-patch antenna mounted on spherical structure

Frequency: 2.0 GHz – 3.0 GHz

The mechanical and dielectric data of the stacked-patch antenna is given in the following tables:

No.of layer	Layer description	Relative permittivity	Loss tangent	Inner radius	Outer radius	Thickness
-	ground sphere	-	-	18.5 cm	18.5 cm	-
1	Dielactric layer (air)	1.0	0.0	18.5 cm	19.02 cm	0.52 cm
2	Dielactric layer (air)	1.0	0.0	19.02 cm	19.54 cm	0.52 cm

Circular stacked-patch element data:

Patch number	Element is printed on	Diameter
1	Outer shell of layer no. 1	6.2 cm
2	Outer shell of layer no. 2	5.45 cm

Coaxial excitation position, relative to patch center: **2.0 cm**

Array configuration: **single-layer patch element.**

Figure 4.19. The comparison of calculated and measured input impedance.

4.3.5 Spherical stacked-patch array of two elements of diameter 6.2 cm

Antenna description

Type: Circular stacked-patch antenna mounted on spherical structure

Frequency: 2.0 GHz – 3.0 GHz

The mechanical and dielectric data of the stacked-patch antenna is given in the following tables:

No.of layer	Layer description	Relative permittivity	Loss tangent	Inner radius	Outer radius	Thickness
-	ground sphere	-	-	18.5 cm	18.5 cm	-
1	Dielactric layer (air)	1.0	0.0	18.5 cm	19.02 cm	0.52 cm
2	Dielactric layer (air)	1.0	0.0	19.02 cm	19.54 cm	0.52 cm

Circular stacked-patch element data:

Patch number	Element is printed on	Diameter
1	Outer shell of layer no. 1	6.2 cm
2	Outer shell of layer no. 2	5.45 cm

Coaxial excitation position, relative to patch center: **2.0 cm**

Array configuration:

Patch center distances	No.of elements	Separation direction
10.25 cm	2	E - plane
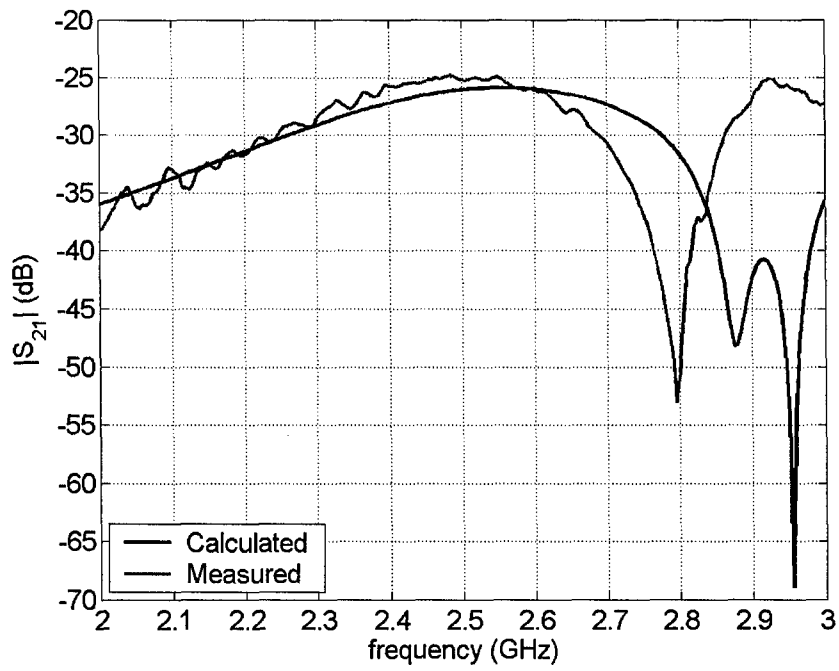
Figure 4.20. Calculated and measured magnitude of S_{21} parameter of a two-patch array.

4.3 Sensitivity of the resonant frequency

Recently, we have made an experimental model to investigate properties of rectangular patch antennas mounted on spherical structures (Fig. 4.21; this effort was supported by the project F61775-01-WE024 where the arrays of single-layer rectangular microstrip patches mounted on spherical structures were fully analyzed). The model was built from a copper sphere of radius $a =$ 18.5 cm on which patches were mounted at different positions. Small styrofoam cubes ($\varepsilon_r \approx 1.0$) were used as spacers between patches and the grounded shell.
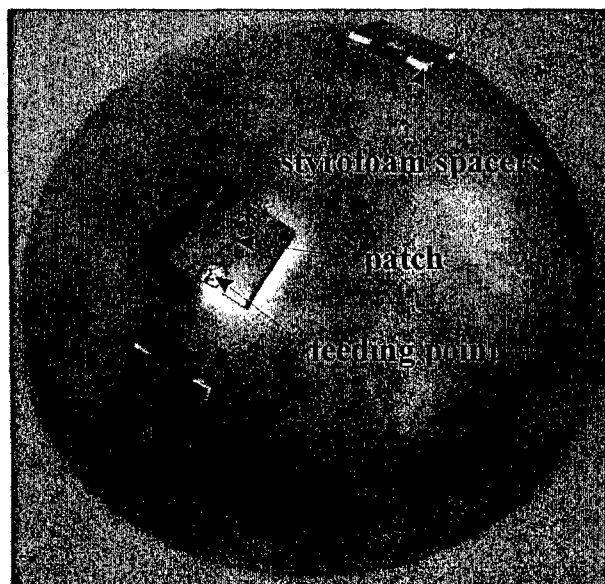
Figure 4.21. Experimental model developed at the University of Zagreb.

To experimentally investigate the influence of the structure curvature on spherical patch properties we have built a spherical patch antenna with large angular width. The patch dimensions are 20×20 cm^2, thickness $h = r_{patch} - r_{gnd} = 0.45$ cm, and the feed point is placed 8.0 cm from the patch center. At the beginning we did not pay too much attention on deviation from the spherical symmetry, i.e. we had made a patch with smaller radius of curvature than required. Consequently, the measured resonant frequency was too low. After correcting the patch radius of curvature we got a very good agreement between calculated and measured results (Fig. 4.22). The calculations were made with the program SMiPA.
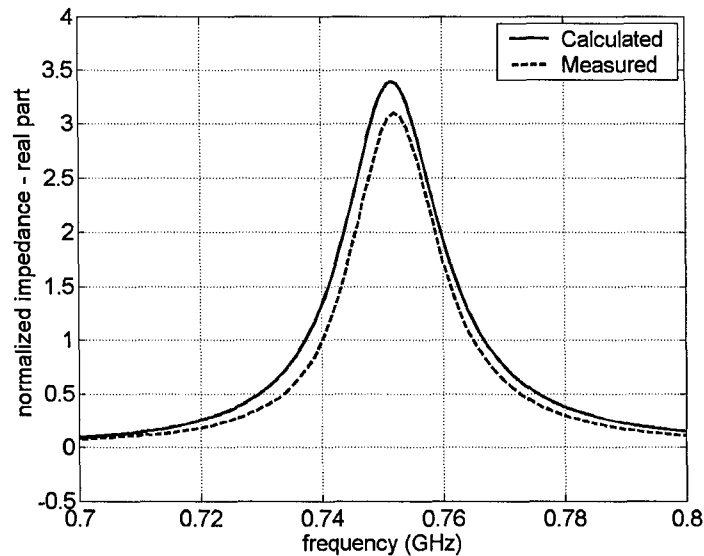
(a)
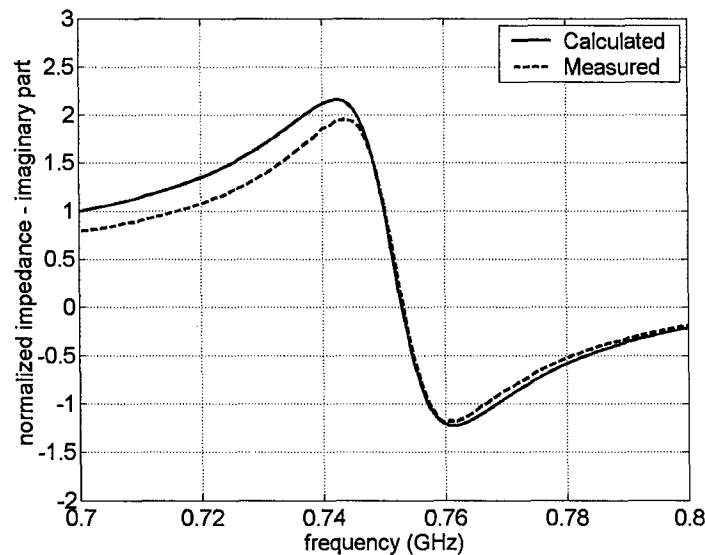
(b)

Figure 4.22. Comparison of calculated and measured input impedance of the 20 x 20 cm^2 patch: (a) real part, (b) imaginary part.

This sensitivity on deviation from the spherical symmetry can be explained using the perturbational method, i.e. one can determine the resonant frequency shift due to the change of the cavity volume [31]. The resonant frequency is directly influenced by the electric and magnetic energies yielded or removed from the cavity:

$$\frac{\omega - \omega_0}{\omega_0} \approx \frac{\iiint\limits_{\Delta V} \left(\mu |\mathbf{H}_0|^2 - \varepsilon |\mathbf{E}_0|^2\right) dV}{\iiint\limits_{V} \left(\mu |\mathbf{H}_0|^2 + \varepsilon |\mathbf{E}_0|^2\right) dV}, \tag{25}$$

where ΔV represents the volume removed from the resonator and the $\mathbf{E}_0$ and $\mathbf{H}_0$ are the electromagnetic field distribution of the unperturbed cavity. To investigate more deeply this sensitivity of spherical patch antennas we have used a commercial program Fidelity based on the FDTD method. Three different configurations for a 20×20 cm^2 patch were analyzed (Fig. 4.23), i.e. the patches have a 0.5 cm too large, correct and 0.5 cm too small curvature, respectively. Results are given in Fig. 4.24, where a large sensitivity of the resonant frequency on spherical symmetry of the patch can be seen. Notice that the average distance of the radiated patch edges from the PEC shell is the same in all three cases, i.e. one would expect that the resonant frequency is almost the same in all three cases since the fringing fields are approximately the same. However, configuration C has a higher resonant frequency since the removed volume is from the middle part of the cavity where the magnetic field has a maximum, while configuration A has a lower resonant frequency since we have added volume to the middle part of the cavity. It is worth mentioning that the developed program is much faster and more accurate than the used commercial FDTD program: the FDTD program needs around 9 hours for calculating one configuration while our program needs only 9 seconds, and the resonant frequency calculated by the FDTD program deviates a lot from the measured one.

The resonant frequency is also sensitive on the structure radius (the resonant frequency is defined as frequency at which the real part of input impedance has the maximum value). In the example shown in Fig. 4.25 patch dimensions were kept constant (20×20 cm^2 patch from table 1 of thickness $h = 0.45$ cm, the feed point placed 8.0 cm from the patch center), and the only parameter that was changed was the structure radius. Therefore, the angular dimensions of the patch were also changed $(2\theta_p = 2\phi_p = W_{patch}/r_{patch}$). Intuitively, one would expect small changes of the resonant frequency comparing to the equivalent planar case. However, these changes are quite big, see Fig. 4.25 where the resonant frequency is obtained both by the moment method and by the cavity model [32]. It can be seen that with increasing the angular dimensions of the patch the resonant frequency also increases. The moment method results are more accurate since fringing fields are not taken into account in the cavity model. Furthermore, the calculated resonant frequency of an equivalent circular-cylindrical patch antenna is also presented in Fig. 7 (the cylindrical patch is ϕ-polarized). It can be seen that the spherical patch antennas are much more sensitive on bending than cylindrical ones. An explanation is that the double-curved structures have more complex resonant mechanism than merely the interference of a forward and a backward propagating wave. The resonant frequency of a planar equivalent patch antenna is 709 MHz (calculated using accurate empirical formulas [33]).

The described properties of the resonant frequency are also valid for circular patch antennas mounted on spherical structures.
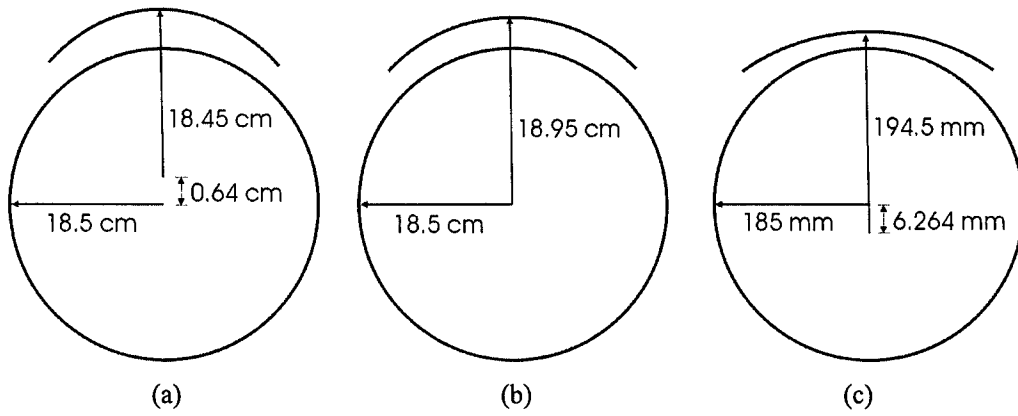
Figure 4.23. Three configuration of a 20 x 20 cm^2 patch antenna with different curvatures.

(a)
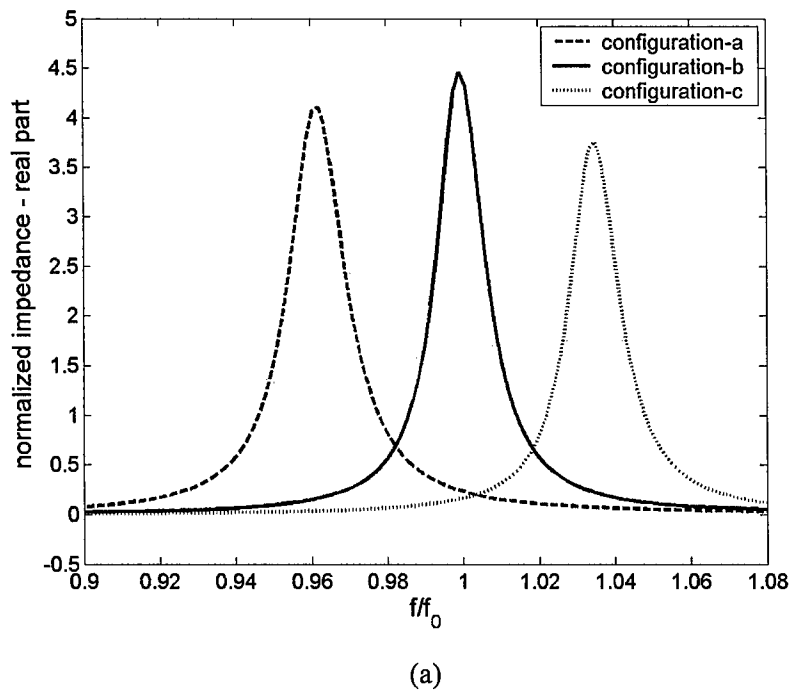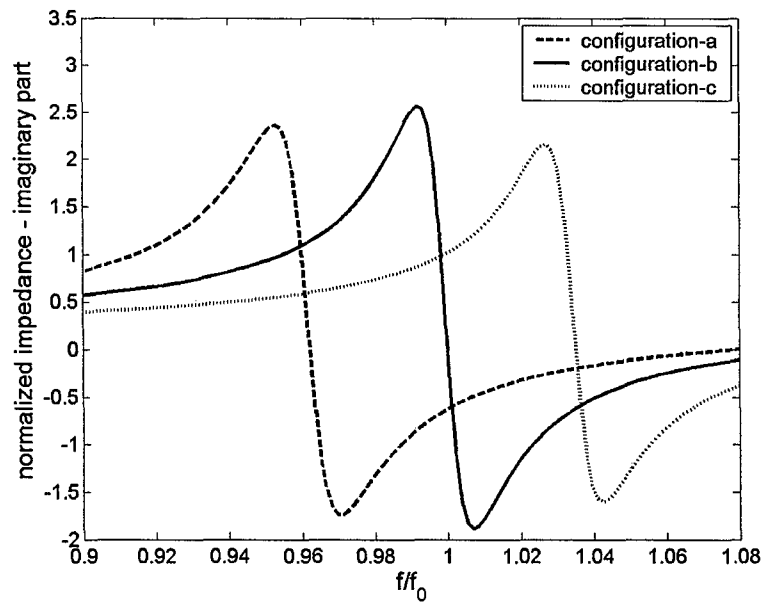
(b)

Figure 4.24. Calculated input impedance of three configurations of a patch antenna with different curvatures (geometry of the structures is given in Fig. 4.23).
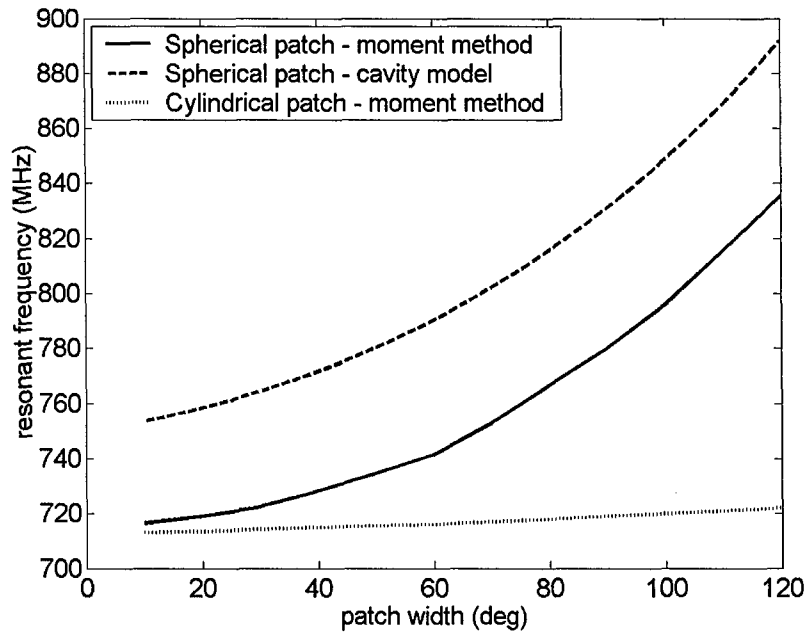
Figure 4.25. Resonant frequency of a spherical rectangular patch antenna as a function of the structure curvature.

4.3.1 Appendix

Cavity model of spherical-rectangular patch antenna

A patch antenna can be modeled as a resonant cavity with PEC walls that represent the patch and the grounded sphere, and with PMC walls which represent the edges of the resonator [28], [13]. Since patch antennas are usually very thin, one can assume that there is only the radial component of the electric field inside the cavity, and that it does not depend on the radial coordinate. Therefore, for $r \cong r_{gnd} \cong r_{patch}$, the E_r field component satisfies the following differential equation

$$\frac{1}{r_{patch}^2 \sin\theta} \frac{\partial}{\partial\theta}\left(\sin\theta \frac{\partial E_r}{\partial\theta}\right) + \frac{1}{r_{patch}^2 \sin^2\theta} \frac{\partial^2 E_r}{\partial\phi^2} + \varepsilon_r k_0^2 E_r = 0. \tag{26}$$

The E_r component of each cavity mode is equal

$$E_r^{v,\mu}(\theta,\phi,r) = \left(a_1 P_v^\mu(\cos\theta) + a_2 P_v^\mu(-\cos\theta)\right) \cos\left(\mu\left(\phi - \frac{W_\phi}{2}\right)\right) \tag{27}$$

The indices v and μ are determined from the boundary conditions that describe the cavity model:

a) $H_\theta = 0$ at $\phi = \pm W_\phi/2$.

From Eq. (A2) we get the condition for μ: $\sin(\mu W_\phi) = 0$.

b) $H_\phi = 0$ at $\theta = \pi/2 \pm W_\theta/2$.

From eq. (A2) we get the conditions for v:

$$\begin{aligned}
a_1 \left.\frac{P_v^\mu(\cos\theta)}{\partial\theta}\right|_{\theta=\pi/2-W_\theta/2} + a_2 \left.\frac{P_v^\mu(-\cos\theta)}{\partial\theta}\right|_{\theta=\pi/2-W_\theta/2} &= 0 \\
a_1 \left.\frac{P_v^\mu(\cos\theta)}{\partial\theta}\right|_{\theta=\pi/2+W_\theta/2} + a_2 \left.\frac{P_v^\mu(-\cos\theta)}{\partial\theta}\right|_{\theta=\pi/2+W_\theta/2} &= 0
\end{aligned} \tag{28}$$

The value of v, i.e. the case when the system (28) has non-trivial solutions a_1 and a_2, is determined from the condition:

$$\begin{vmatrix} \dfrac{P_v^\mu(\cos\theta)}{\partial\theta}\bigg|_{\theta=\pi/2-W_\theta/2} & \dfrac{P_v^\mu(-\cos\theta)}{\partial\theta}\bigg|_{\theta=\pi/2-W_\theta/2} \\[2ex] \dfrac{P_v^\mu(\cos\theta)}{\partial\theta}\bigg|_{\theta=\pi/2+W_\theta/2} & \dfrac{P_v^\mu(-\cos\theta)}{\partial\theta}\bigg|_{\theta=\pi/2+W_\theta/2} \end{vmatrix} = 0. \qquad (29)$$

The resonant frequency is obtained after putting the expression for the E_r component of the resonant mode (27) into the equation (26)

$$f^{v,\mu} = \frac{c}{2\pi\sqrt{\varepsilon_r}}\frac{\sqrt{v(v+1)}}{r_{patch}}. \qquad (30)$$

5   BENCHMARKS

5.1 Return loss of spherical stacked-patch antenna

5.1.1 Introduction

This example deals with the return loss (S_{11} parameter) of a circular stacked-patch antenna embedded in a multilayer spherical structure. The geometry of the problem is given in Figure 5.1. The fed circular patch has a diameter of 2.647 cm, the parasitic patch has a diameter of 2.779 cm, and the antenna is embedded in a multilayer structure consisting of two substrates with $\varepsilon_r = 2.45$ separated by a foam with dielectric constant $\varepsilon_r = 1.22$.

The detailed data sheet about the calculated/measured antenna is given in 5.2.2. In order to calculate this example a run of SMiSPA is needed, with an input file that is shown in section 6.4.3. The calculated results are compared with measured results of the planar counterpart [29].
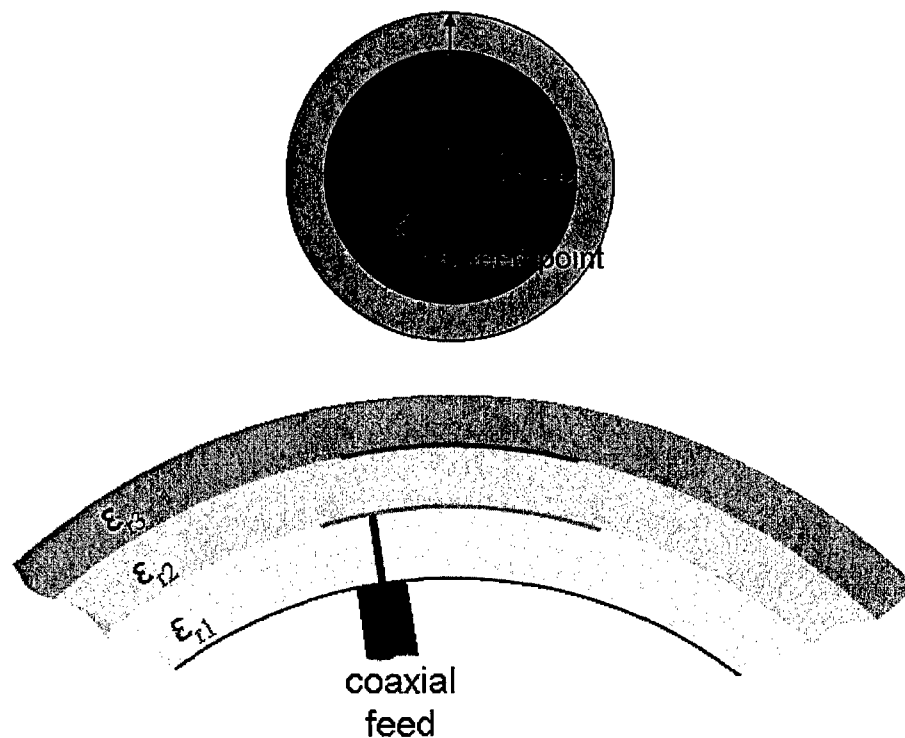
Figure 5.1. The geometry of one circular stacked-patch antenna

5.1.2 Summary - technical description

Antenna / Antenna Array description

Type: Circular stacked-patch element embedded in spherical multilayer substrate

Frequency: 3.0 GHz – 5.5 GHz

The mechanical and dielectric data of the structure (first case of interest):

no.of layer	layer description	relative permittivity	loss tangent	inner radius	outer radius	thickness
-	ground sphere	-	-	planar	planar	-
1	Dielactric layer	2.45	0.001	planar	planar	0.152 cm
2	Foam layer	1.22	0.0001	planar	planar	0.4764 cm
3	Dielactric layer	2.45	0.001	planar	planar	0.0761 cm

no.of layer	layer description	relative permittivity	loss tangent	inner radius	outer radius	Thickness
-	ground sphere	-	-	20 cm	20 cm	-
1	Dielactric layer	2.45	0.001	20.0 cm	20.152 cm	0.152 cm
2	Foam layer	1.22	0.0001	20.152 cm	20.6284 cm	0.4764 cm
3	Dielactric layer	2.45	0.001	20.6284 cm	20.7045 cm	0.0761 cm

Circular stacked-patch element data:

Patch number	Element is printed on	diameter
1	outer shell of layer no. 1	2.647 cm
2	outer shell of layer no. 2	2.779 cm

Coaxial excitation position, relative to patch center: **0.794 cm**

Array configuration: **single element**

5.1.3 Numerical and experimental results

The calculation is performed in frequency range of 3.0 to 5.5 GHz at 91 equidistant frequency points. Figure 6.15 shows the input file for the program SMiSPA. Light printed are the values and rows that are irrelevant for this case. Here, distance between patches is irrelevant since a single patch configuration is considered. Additionally, all data for radiation pattern is irrelevant, since in this benchmark only the input impedance is of interest.

```
3.2      5.0      91      R ! Frequency (GHz)
20.0                        ! Ground shell and patch radius (cm)
3                           ! Number of dielectric layers
0.152    2.45    0.001      ! Relative permittivity and loss tanges
0.4764   1.22    0.0001     ! Relative permittivity and loss tanges
0.0761   2.45    0.001      ! Relative permittivity and loss tanges
1        2                  ! Die. layer at which patches are placed
1        1        R         ! Array grid parameters and grid type
2.647    2.779    C         ! Patch diameter(cm),circular shape
C                           ! Feeding type:'c'=coax,'m'=microstrip,'a'=apertu
1                           ! Number of ports per patch
0.794    0.0                ! Port position
Y                           ! Equal port excitations? (Y - yes, N - no)
0.0      0.0                ! Distance between patch centers
50.0                        ! Characteristic impedance of the feed line
-180.0   180.0    361       ! Azimuthal pattern
-89.0    269.0    359       ! Elevation pattern
0.0                         ! Phi angle of the evelation pattern
90.0     0.0                ! Theta and phi angle of the main beam
L                           ! Polarization (L - linear, C - circular)
1                           ! Phase corrected excitation
```

Figure 5.2. Input file *smispa.in* for 0.4764 cm thickness of the foam layer.

Notice that the second case differs only in the thickness of the foam layer (h_2 = 0.6352 cm instead of h_2 = 0.4764 cm). In other words, the mechanical and dielectric data of the structure for the second case of interest is:

no.of layer	layer description	relative permittivity	loss tangent	inner radius	outer radius	Thickness
-	ground sphere	-	-	20 cm	20 cm	-
1	Dielactric layer	2.45	0.001	20.0 cm	20.152 cm	0.152 cm
2	Foam layer	1.22	0.0001	20.152 cm	20.7872 cm	0.6352 cm
3	Dielactric layer	2.45	0.001	20.7872 cm	20.8633 cm	0.0761 cm

The comparison of the calculated and measured magnitude of S_{11} parameter is given in Figures 5.3 and 5.4. The measured results are for the planar equivalent case [29].
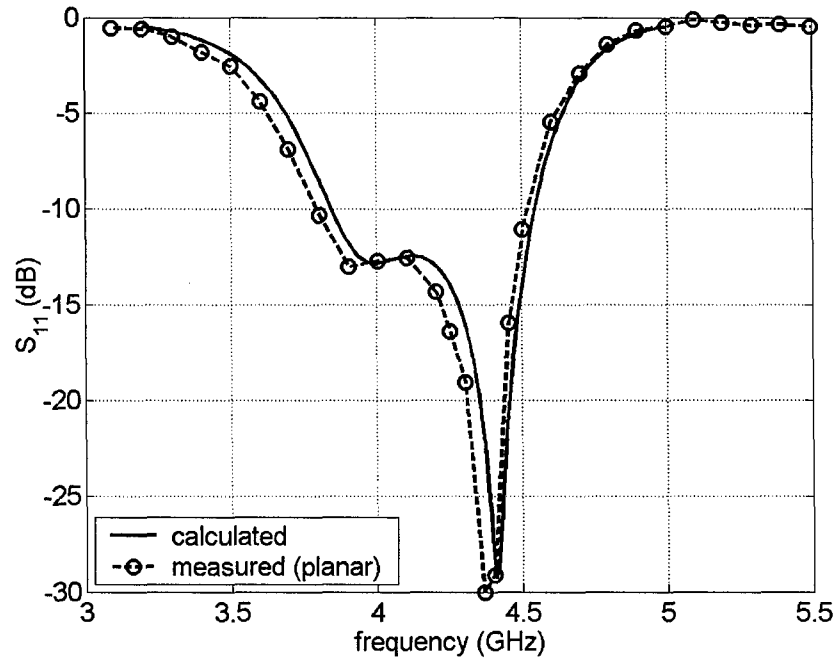
Figure 5.3. Comparison of the calculated magnitude of S_{11} parameter with measurements of the planar case ($h_2 = 0.6352$ cm).
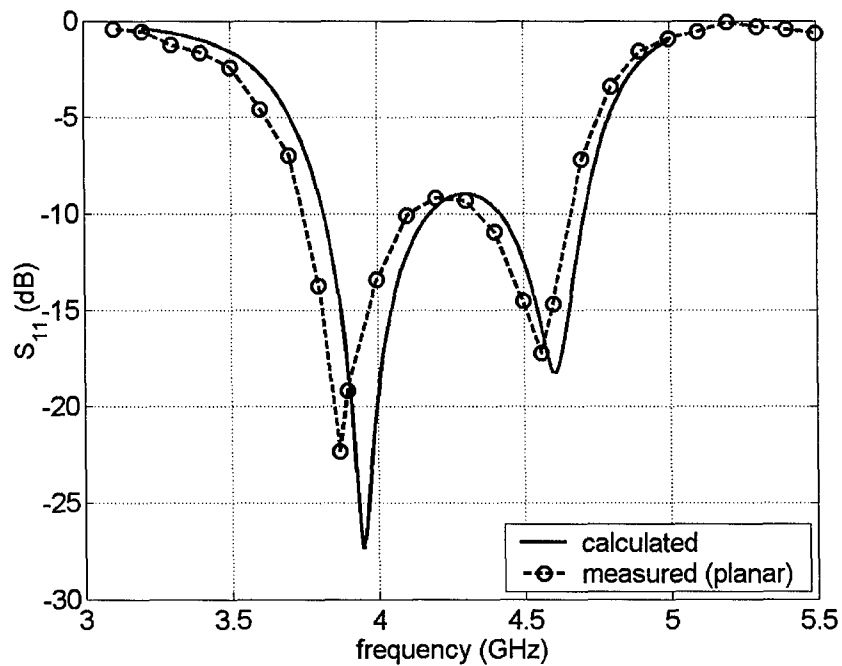

Figure 5.4. Comparison of the calculated magnitude of S_{11} parameter with measurements of the planar case ($h_2 = 0.4764$ cm).

5.2 Input impedance of spherical stacked-patch antenna

5.2.1 Introduction

This example deals with the input impedance of a circular stacked-patch antenna embedded in a multilayer spherical structure. The geometry of the problem is the same as in the previous example, i.e. it is given in Figure 5.1. The only difference is in the size of the patch radiators: the fed circular patch has a diameter of 2.647 cm and the parasitic patch has a diameter of 2.673 cm. Like in the previous case, the calculated results are compared with the measured results of the planar counterpart [29].

5.2.2 Numerical and experimental results

Antenna / Antenna Array description

Type: Circular stacked-patch element embedded in spherical multilayer substrate

Frequency: 3.2 GHz – 5.0 GHz

The mechanical and dielectric data of the structure (first case of interest):

no.of layer	layer description	relative permittivity	Loss tangent	inner radius	outer radius	thickness
-	ground sphere	-	-	planar	planar	-
1	Dielactric layer	2.45	0.001	planar	planar	0.152 cm
2	Foam layer	1.22	0.0001	planar	planar	0.4764 cm
3	Dielactric layer	2.45	0.001	planar	planar	0.0761 cm

no.of layer	layer description	relative permittivity	Loss tangent	inner radius	outer radius	Thickness
-	ground sphere	-	-	20 cm	20 cm	-
1	Dielactric layer	2.45	0.001	20.0 cm	20.152 cm	0.152 cm
2	Foam layer	1.22	0.0001	20.152 cm	20.6284 cm	0.4764 cm
3	Dielactric layer	2.45	0.001	20.6284 cm	20.7045 cm	0.0761 cm

Circular stacked-patch element data:

Patch number	Element is printed on	Diameter
1	Outer shell of layer no. 1	2.647 cm
2	Outer shell of layer no. 2	2.673 cm

Coaxial excitation position, relative to patch center: 0.794 cm
Array configuration: single element

The comparison of the calculated and measured input impedance is given in Figures 5.5 and 5.6. The measured results are for the planar equivalent case [29].
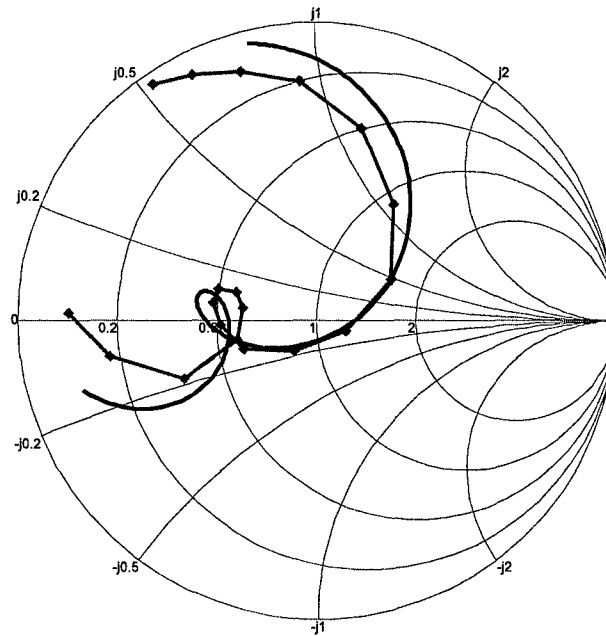
*Figure 5.5.* Comparison of the calculated input impedance with measurements of the planar case (h_2 = 0.4764 cm); — calculated results, ◊ measured results.
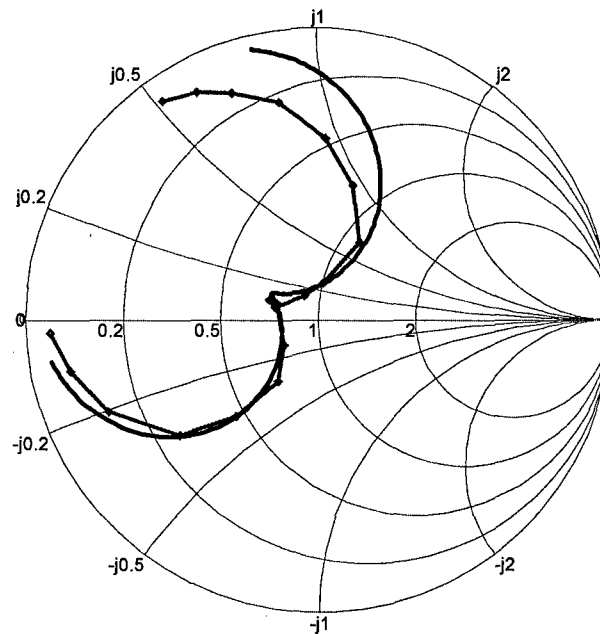
*Figure 5.6.* Comparison of the calculated input impedance with measurements of the planar case (h_2 = 0.6352 cm); — calculated results, ◊ measured results.

5.3 Radiation pattern of spherical stacked-patch antenna

5.3.1 Introduction

In this example we consider the effect of the radius of the ground plane (grounded shell) on radiation pattern of a circular stacked-patch antenna embedded in a multilayer spherical structure. For comparison, the calculated radiation pattern of the planar patch antenna with same dimensions is also given. The geometry of the problem is the same as in the previous examples, i.e. it is given in Figure 5.1. The fed circular patch has a diameter of 2.647 cm, the parasitic patch has a diameter of 2.673 cm, and the thickness of the foam layer is $h_2 = 0.6352$ cm. The operating frequency is 4.5 GHz. It can be seen that with enlarging the radius of the sphere the main lobe of the spherical patch antenna approaches the main lobe of the planar counterpart. As expected, the back-radiation is smaller for spheres with larger radius.

5.3.2 Numerical results

<u>Antenna / Antenna Array description</u>

Type: Circular stacked-patch element embedded in spherical multilayer substrate

Frequency: 4.5 GHz

The mechanical and dielectric data of the structure:

no.of layer	layer description	relative permittivity	loss tangent	inner radius	outer radius	thickness
-	ground sphere	-	-	planar	planar	-
1	Dielactric Layer	2.45	0.001	planar	planar	0.152 cm
2	Foam Layer	1.22	0.0001	planar	planar	0.6352 cm
3	Dielactric Layer	2.45	0.001	planar	planar	0.0761 cm

no.of layer	layer description	relative permittivity	loss tangent	inner radius	outer radius	Thickness
-	ground sphere	-	-	20 cm	20 cm	-
1	Dielactric layer	2.45	0.001	20.0 cm	20.152 cm	0.152 cm
2	Foam layer	1.22	0.0001	20.152 cm	20.7872 cm	0.6352 cm
3	Dielactric layer	2.45	0.001	20.7872 cm	20.8633 cm	0.0761 cm

Circular stacked-patch element data:

Patch number	Element is printed on	Diameter
1	outer shell of layer no. 1	2.647 cm
2	outer shell of layer no. 2	2.673 cm

Coaxial excitation position, relative to patch center: **0.794 cm**
Array configuration: **single element**

The comparison of the calculated radiation patterns in *H*- and *E*-planes for spherical structures with different radii is given in Figures 5.7 and 5.8.
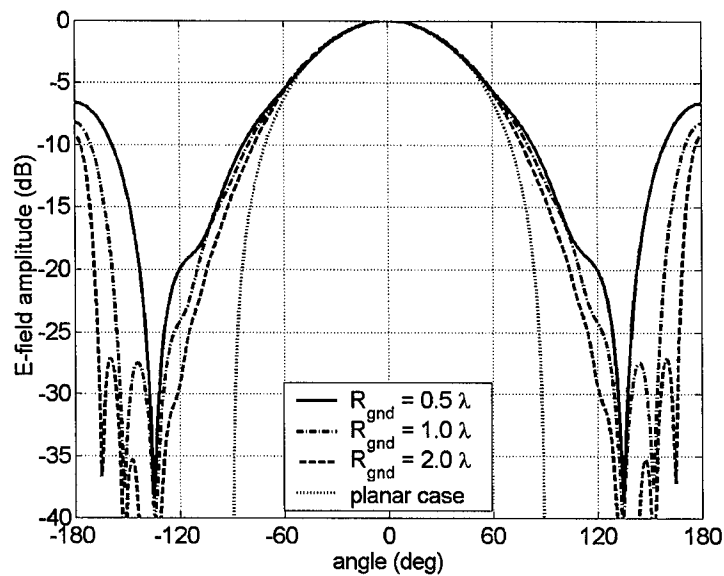

Figure 5.7. Radiation pattern in *H*-plane of a spherical rectangular patch antenna for different sphere radii.
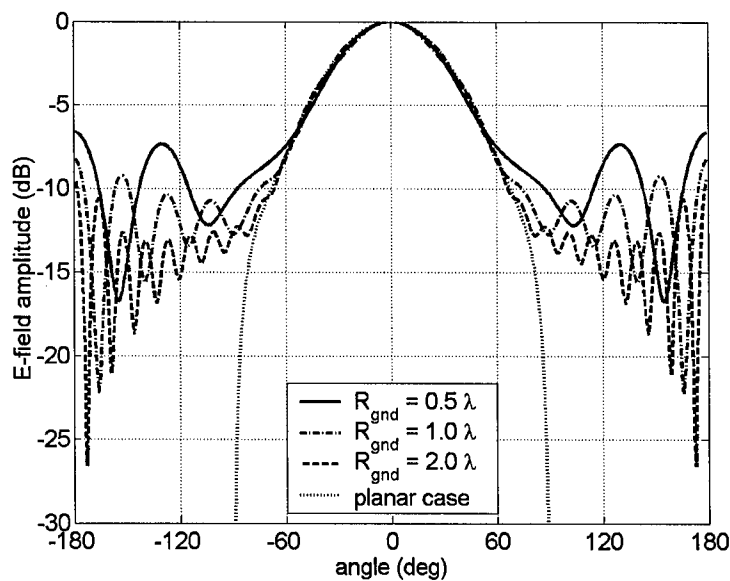

Figure 5.8. Radiation pattern in *E*-plane of a spherical rectangular patch antenna for different sphere radii.

**5.4 Mutual coupling of two circular patches
printed on spherical structure**

5.4.1 Introduction

This example deals with mutual coupling of two circular patch antennas printed on spherical structure (unfortunately, in open scientific literature there are no measured results of mutual coupling between circular stacked-patch antennas). The geometry of the problem is given in Fig. 5.9. The circular patches of a diameter 1.86 cm are printed on a grounded dielectric layer (ε_r = 12.5, h_l = 0.16 cm). The influence of the sphere radius on mutual coupling level is shown in Figs. 5.10 and 5.11 where the magnitude of the S_{21} parameter, both in E- and H-plane, is shown as a function of spacing between patch edges. The coupling level is compared to the measured results of equivalent planar case [30]. The operating frequency of planar patches is 5.6375 GHz, while in spherical case the operating frequency is changed a bit in order to obtain good matching The detailed data sheet about the calculated/measured antenna is given in 5.4.2. The comparison of calculation and measurement can be found in section 5.4.2 as well. The mutual coupling is weaker in spherical case (compared to the planar case) in both E- and H-planes, and it decreases more rapidly when the spacing between patches is increased. For smaller structure radii mutual coupling starts to be oscillatory due to interference of forward and backward propagating waves around the sphere.
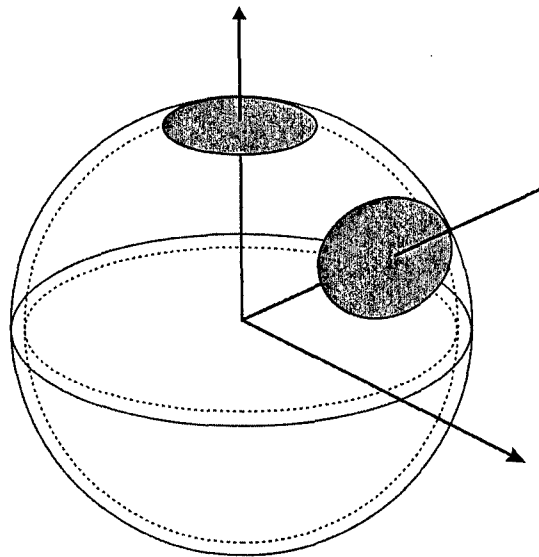
Figure 5.9. Two element array of circular patches on spherical structure.

5.4.2 Numerical and experimental results

Antenna / Antenna Array description

Type: Circular patch elements printed on a spherical grounded substrate.

Frequency: 5.6375 GHz

The mechanical and dielectric data of the structure ($R_{gnd} = 2\ \lambda$):

no.of layer	layer description	relative permittivity	loss tangent	inner radius	outer radius	thickness
-	ground sphere	-	-	10.643 cm	10.643 cm	-
1	Dielactric layer	2.5	0.002	10.643 cm	10.803 cm	0.16 cm

Circular stacked-patch element data:

Patch number	Element is printed on	Diameter
1	outer shell of layer no. 1	1.86 cm

Coaxial excitation position, relative to patch center: **0.794 cm**

Array configuration:

patch center distances	no.of elements	separation direction
variable	2	θ (azimuthal)

The comparison of the calculated and measured magnitude of the S_{21} parameter is given in Figures 5.10 and 5.11. The measured results are for the planar equivalent case [30].

Figure 5.10. Calculated magnitude of S_{21} parameter of a two-patch array as a function of spacing between patch centers; E-plane coupling.

The mechanical and dielectric data of the structure ($R_{gnd} = 2\ \lambda$):

no.of layer	layer description	relative permittivity	loss tangent	inner radius	outer radius	thickness
-	ground sphere	-	-	10.643 cm	10.643 cm	-
1	Dielactric layer	2.5	0.002	10.643 cm	10.803 cm	0.16 cm

Circular stacked-patch element data:

Patch number	Element is printed on	Diameter
1	outer shell of layer no. 1	1.86 cm

Coaxial excitation position, relative to patch center: 0.794 cm

Array configuration:

patch center distances	no.of elements	separation direction
variable	2	θ (azimuthal)

The comparison of the calculated and measured magnitude of the S_{21} parameter is given in Figures 5.10 and 5.11. The measured results are for the planar equivalent case [30].

Figure 5.10. Calculated magnitude of S_{21} parameter of a two-patch array as a function of spacing between patch centers; *E*-plane coupling.

*Figure 5.11.* Calculated magnitude of S_{21} parameter of a two-patch array as a function of spacing between patch centers; H-plane coupling.

6 PROGRAM SMiSPA

6.1 Introduction to SMiSPA

6.1.1 Introduction

This chapter gives the user's manual for the program SMiSPA. The abbreviation SMiSPA means the program for analyzing Spherical Microstrip Stacked-Patch Arrays. Since there are different requirements on calculation of radiation pattern and input impedance/mutual coupling, we have actually developed two programs SMiSPA and SMiSPApat. The main reason for splitting the problem into two parts is that radiation pattern is usually calculated only for one frequency, while input impedance and mutual coupling is usually calculated for frequency band of interest (and thus even hundreds of frequency points can be calculated). Therefore, program SMiSPA calculates

- current distribution at each patch in the array

- input impedance at each input port in the array

- mutual coupling between each two patches in the array

and program SMiSPApat calculates

- radiation pattern of the array without taking mutual coupling into account

- radiation pattern of the array when all mutual couplings are taken into account.

Program is written in FORTRAN 90, and therefore can be compiled and run at each machine where FORTRAN 90 is installed or which support the executable version of the program. The communication with the program is made via input/output ASCII files. For case of simplicity, both programs SMiSPA and SMiSPApat are using the same input file (smipa.in). The detailed description of input and output files are given in this chapter.

We have also developed a graphical user interface, called SMiPAwin, for IBM PC compatible computers under Windows operating system (the description of SMiPAwin is given in the report F61775-01-WE024 "Analysis of Curved Microstrip Antennas"). By this it is easier to define the input parameters, and to obtain graphical presentation of the results. Programs SMiSPA and SMiSPApat are working independently of graphical user interface, i.e., graphical user interface is used only for writing the input file, running the SMiSPA and SMiSPApat programs, reading the

output files, and displaying the results. The same graphical user interface is used for running previously developed programs SMiPA and SMiPApat.

6.1.2 Problem Domain Description

The SMiSPA and SMiSPApat programs analyze microstrip stacked-patch antennas or antenna arrays placed on spherical structures, as illustrated in Fig. 6.1. If an array is analyzed, following assumptions are made:

- all antenna elements are identical, both in terms of dimensions, shape and feed/port types

- the patch elements are of circular shape

- the dielectric structure can be multilayered with losses

- the patch array must be placed at the top of one such layer

- two types of feeding structures can be analyzed: coax feeding and microstrip line feeding

- multiple ports can be defined on patch, e.g. when designing circularly polarized arrays.

By means of SMiSPA program current distribution at each patch in the array can be calculated, as well as input impedance at each input port and mutual coupling between each two patches. The SMiSPApat program calculates then radiation pattern of the array, with or without taking mutual coupling into account.
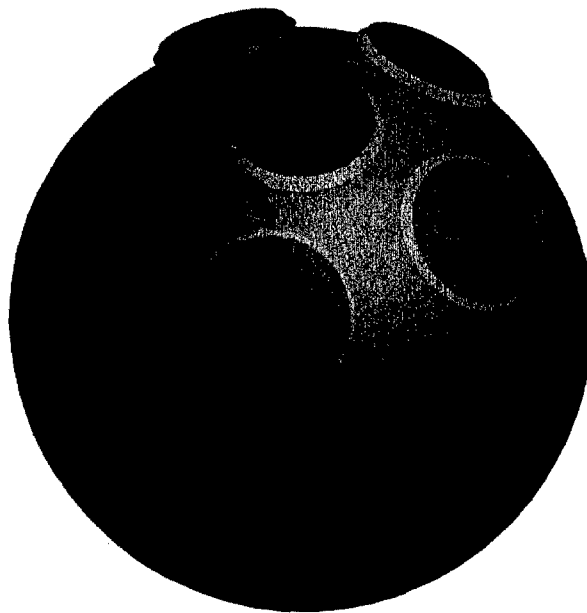
Figure 6.1. The geometry of the spherical patch array

6.1.3 Text File Interface

The programs SMiSPA and SMiSPApat interact with the user and with each other using ASCII text files. This scheme, with all files in question is presented in Fig. 6.2. Similar input and output files with the same names are used for running previously developed programs SMiPA and SMiPApat.
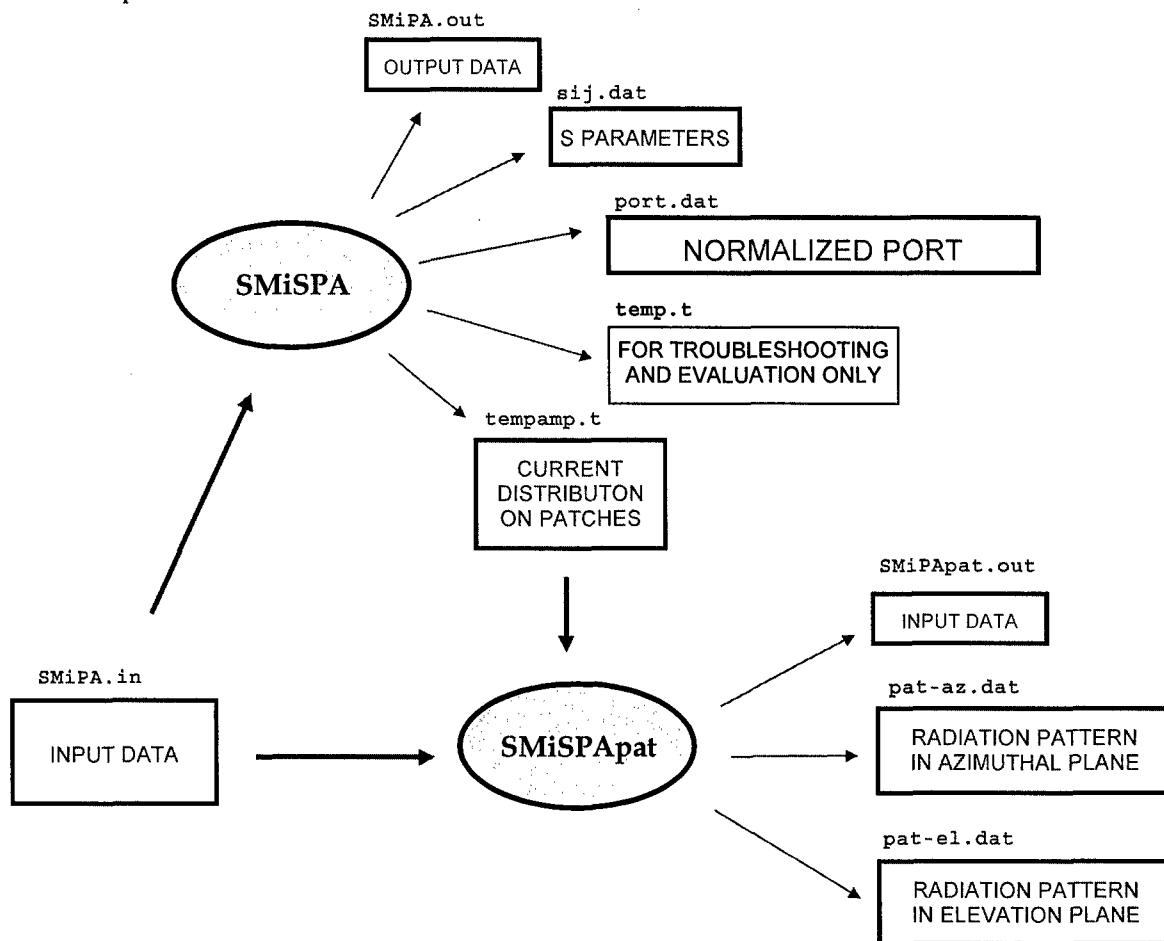
Figure 6.2. Input and output files for the programs SMiSPA and SMiSPApat.

The program can calculate the following antenna characteristics:

(a) current distribution at each patch in the array

(b) input impedance of each patch in the array

(c) mutual coupling between each two patches in the array

(d) radiation pattern of the array when all mutual couplings are taken into account

(e) radiation pattern of the array without taking mutual coupling into account (fast calculations of the radiation pattern are needed for making first design of the array).

6.1.3.1 The SMiPA.in file

The name of the input file for both SMiSPA and SMiSPApat programs is **SMiPA.in**. Each line possesses the value of several variables and short description of these variables. Since our intention was to make a compatible program with previously developed programs SMiPA/SMiPApat we have decided to use the input out files with the same names and structures. The parts of the input/output files that have different meaning are written in bold letters. The input variables, which must have values when the call of the SMiSPA and SMiSPApat is made, are:

First line:

Fmin, Fmax, Nfrequency,Modecal   REAL, REAL, INTEGER, CHARACTER

Fmin and *Fmax* are the minimum and maximum frequency (in GHz). *Nfrequency* is the number of frequency points for which the array is analyzed. These values are used only when the call of the SMiSPA program is made. SMiSPApat program calculates the radiation pattern only for one frequency, and that frequency is *Fmin*. If we first calculate the patch currents at *Nfrequency* frequency points (by calling SMiSPA program), then we can choose the frequency point for which we want to calculate the radiation pattern by choosing *Fmin*. The only condition is that the patch currents are calculated for the chosen frequency point. *Modecal* represents the calculation mode – R means accurate (rigorous) mode suggested for final design, and F means less-accurate (fast-design) mode suggested for first design.

Second line:

R_{GND} REAL

R_{GND} is the radius of the grounded tube (in cm).

Third line:

Nlayer   INTEGER

Nlayer is the number of dielectric layers.

Next *Nlayer* lines:

h, EpsilonR, Tdelta   REAL

Each line contains three parameters: *h, EpsilonR* and *Tdelta* which describe the thickness, the relative permittivity and loss tangent of each dielectric layer, respectively.

Next line:

Npatlayer, Nspatlayer   INTEGER

Npatlayer and **Nspatlayer** are the numbers of the dielectric layer at top of which the patches are placed. In other words, the lower patches are placed between dielectric layers **Npatlayer** and **Npatlayer+1**, and the upper patches are placed between dielectric layers **Nspatlayer** and **Nspatlayer+1**. If the

patches are placed in the middle of some dielectric layer, an additional dielectric layer should be introduced, i.e. the considered dielectric layer should be split into two parts and the patches should be placed at the interface between these two dielectric layers.

Next line:

Npat1, Npat2, Lattice	INTEGER, CHARACTER

Lattice represents the type of the grid lattice – R means rectangular lattice, I means icosahedron lattice, and F means that the position of each patch is read at the end of the input file. For rectangular lattice *Npat1* and *Npat2* are the number of patches in the θ- and ϕ-directions, respectively. For icosahedron lattice *Npat1* is the number of rings in the array, and *Npat2* denotes the ratio between the sides of equilateral triangles of the icosahedron structure and of the considered array (for example, in Fig. 4.6 *Npat1*=3 and *Npat2*=4). If the patch position is read from the file, then *Npat1* and *Npat2* have no meaning and therefore they can have arbitrary values.

Next line:

Dpat1, Dpat2, Patshape	REAL, CHARACTER

Dpat1 and **Dpat2** denote the lower and upper patch diameter (in cm), respectively. **Patshape** represents the type of the patch shape: **C** means circular shape (program SMiSPA can analyze only circular patches; for rectangular patches we have developed previously program SMiPA).

Next line:

Modefeed	CHARACTER

Modefeed denotes the type of the patch feeding. M or m means microstrip line feeding, C or c means coax feeding.

Next line:

Nport	INTEGER

Nport denotes the number of ports per patch (i.e. how many ports has each patch).

Next *Nport* lines:

Feedth, Feedphi	REAL

Feedth and *Feedphi* determine the position of the feeding line (in cm) in the local spherical coordinate system, i.e. *Feedth* and *Feedphi* are the θ- and ϕ-coordinates of the feed point, respectively. Note that the z-axis of the coordinate system goes through the center of the patch.

Next line:
Modeexci   CHARACTER

Modeexci determines if the ports have equal excitations, both in amplitude and phase. *Y* or *y* means that the ports are equally excited, *N* or *n* means that the excitations are read at the end of the input file SMiPA.in.

Next line:
Dpatth, Dpatphi   REAL

In the case of rectangular array grid (i.e. if the variable *Lattice* is equal *R*) *Dpatth* and *Dpatphi* are the distances between centers of the patches (in cm) in the θ- and ϕ-directions, respectively. If the variable Lattice is equal *I* or *F*, *Dpatth* and Dpatphi can be arbitrary numbers

Next line:
Z0   REAL

Z0 is the characteristic impedance of the input transmission line (either microstrip or coax line).

The next six lines are needed only when the call of the SMiSPApat program is made. They are:

Phimin, Phimax, Nphi   REAL, REAL, INTEGER

The minimum and maximum angles of ϕ (in deg) in the azimuthal plane, and the number of points which are calculated in the azimuthal pattern, respectively. The azimuthal plane is defined by $\theta = 90^0$ (the coordinate system is in Fig. 1).

Thetamin, Thetamax, Ntheta   REAL, REAL, INTEGER

The minimum and maximum angles of θ (in deg) in the elevation plane, and the number of points which are calculated in the elevation pattern, respectively.

Phiel   REAL

The ϕ angle of the elevation plane (in deg). In other words, the elevation plane is defined by $\phi = Phiel$.

Theta0, Phi0   REAL

The values of the θ and ϕ coordinates (in deg) of the main beam, respectively. The E-field values of the radiation pattern are normalized by the amplitude of the E-field with *Theta0* and *Phi0* coordinates. Furthermore, *Theta0* and *Phi0* values are needed when *Nmode* = 4 (see definition of the *Nmode*), and they are used for determining the phase correction of the current on each patch. By using this phase correction the fields from each patch are in phase in the (*Theta0*, *Phi0*) direction.

Typepolar   CHARACTER

Typepolar denotes the type of polarization of radiation pattern. *L* or *l* means linear polarization, *C* or *c* means circular polarization.

Nmode   INTEGER

Nmode is the mode of calculating the radiation pattern. *Nmode*=0,1 and 5 means that the radiation pattern is calculated rigorously, i.e. the results from the SMiSPA program are used (the calculated current distribution is used for chosen frequency point, see explanation of *Fmin*). *Nmode*=0 means calculation of the gain pattern, *Nmode*=1 means that the radiation pattern is normalized to the reference direction, and *Nmode*=5 means calculation of the element pattern. *Nmode* 2, 3 and 4 means that the radiation pattern is calculated in a simple way, i.e., mutual coupling is not taken into account in calculations of the radiation pattern. When *Nmode* = 2 it is supposed that patch currents have equal amplitudes and phases on each patch. When *Nmode* = 3 amplitudes and phases of each patch current are read from the input file 'SMiPApat.in'. When *Nmode* = 4 all patches have the same amplitude of the current. The phase is corrected in the way that contributions from all patches are in phase in the direction of the main beam, i.e., in the (*theta0, phi0*) direction. If *Nmode*=5, then the number of the patch in the ϕ- and *z*-directions, as well as the port number should be also given in the same line. In that case we need to write additional three integer numbers-coordinates).

The last part of the input file is used in three cases: if the array grid is neither icosahedron nor rectangular, if the ports do not have equal excitations and we want to run SMiSPA program, and if we want to calculate the radiation pattern (SMiSPApat program) by using the simple method and by selecting the amplitudes and phases of currents on each patch (*Nmode* = 3). In all cases the amplitudes and phases of the excitation currents, as well as patch positions, are read from the end of the input file SMiPA.in. The number of lines in the file is the same as the number of patches times number of ports. Each line has 5 numbers: first two numbers are the patch number-coordinates, the third one is the number of the port of the considered patch, and the fourth and the fifth number in each line are the amplitude and the phase of the excitation connected to the considered port of the patch.

For rectangular grid the patch number-coordinates are the number of the patch in θ- and ϕ direction (the patch number of the lowest most left patch is (1,1)). For icosahedron grid the patch number-coordinates are the number of the circle and the number of the patch along the circle. For non-rectangular grid first two numbers represent the patch position (θ and ϕ coordinate in degrees). We can check if these last lines are correctly given by checking the description of the array given in the output files SMiPA.out and SMiPApat.out. If we consider some other case (e.g. if the ports have equal excitations) there is no need for these input data. Therefore:

If needed, next *Npat* x *Nport* lines after one blank line are:

Ipat1, Ipat2, Iport, Amp, Phase   INTEGER, REAL

Ipatphi, *Ipatz*, *Iport* are integers which represents the coordinates of each port (coordinate *Iport*) connected to each patch (coordinates *Ipat1*, *Ipat2*). For that port real numbers *Amp* and *Phase* denote the amplitude and the phase of the excitation current.

or

Thetapat, Phipat, Iport, Amp, Phase   REAL, INTEGER, REAL

Thetapat and *Phipat* represent the θ and ϕ coordinate (in degrees) of the center of each patch, Iport is the number of the patch port, and *Amp* and Phase denote the amplitude and the phase of the excitation current.

6.1.3.2 Description of the output files

There are six output files: 'SMiPA.out', 'SMiPApat.out', 'Sij.dat', 'port.dat' 'pat-az.dat' and 'pat-el.dat', and in them we can find data about the geometry as well as the calculated values of the input impedance, S-parameters and radiation pattern in the elevation and azimuthal planes.

SMiPA.out The file contains data about the input impedance of a single patch (S parameters for array case are given in Sij.dat). When constructing the array we need first to determine the parameters of a single patch, e.g. input impedance, return loss, and impedance bandwidth. The structure of the SMiSPA program (and output file 'SMiPA.out') enables these calculations. First part of the file contains the values of the input file. Therefore the first part looks similar to the input file 'SMiPA.in'. The second part contains the input impedance and return loss for all calculated frequencies. Each line is for one frequency point, and it has four values: frequency (in GHz), normalized input impedance (real and imaginary part) and return loss (in dB). The calculated input impedance is normalized by the characteristic impedance of the feeding transmission line Z0 (the value of Z0 is given in the file 'SMiPA.in'; for aperture-coupled patch antennas it is calculated from the geometry of feeding structure).

SMiPApat.out The file contains data about the array geometry. The first part of the file contains the values of the input file. Therefore the first part looks similar to the input file 'SMiPA.in'. The second part describes the array that is analyzed. It is a list of the all patch elements in the array with their coordinates and amplitude and phase of the patch current. First two columns are the patch number-coordinates, the third column is the number of the basis function on the considered patch, and the forth and fifth columns are the θ- and ϕ-coordinate of the patch. The sixth and seventh columns are the amplitude and phase (in deg) of the considered basis function, respectively.

Sij.dat The file contains the calculated S-parameters. The file is in the Touchstone format, i.e., using this file it is possible to connect SMiSPA and Touchstone programs. The first line is a specification line: '# GHz S DB R' and at the end of the line there is a value of the normalization impedance. GHz means that the frequency values are in GHz, DB means that S-parameters are

written in the dB-angle format. Other lines in the file are the S-parameters for different frequencies. If we have one port (one patch) then each line contains frequency, $|S_{11}|$ in dB, and angle of S_{11}, respectively. In the case of two ports (two patches) each line contains frequency, $|S_{11}|$ in dB, angle of S_{11}, $|S_{21}|$ in dB, angle of S_{21}, $|S_{12}|$ in dB, angle of S_{12}, $|S_{22}|$ in dB, and angle of S_{22}, respectively. In the case of N ports each frequency is described with N lines, each containing $|S_{i1}|$ in dB, angle of S_{i1}, $|S_{i2}|$ in dB, angle of S_{i2}, etc. Frequency is written at the beginning of the first of N lines.

port.dat The file contains the calculated port impedances for each port. For each frequency point port impedances are given in the form of real and imaginary part. The values of port impedances are normalized, i.e. port impedances are divided by Z0.

pat-az.dat   The file contains the field values in the azimuthal plane (the azimuthal plane is defined by $\theta=90^{0}$). The input values of variables *Phimin*, *Phimax* and *Nphi* determine the ϕ values in the azimuthal plane for which the radiation pattern is calculated. The field values are normalized with the field value with *Theta0* and *Phi0* coordinates that are defined in the input file (the exception is for *Nmode* = 0 and *Nmode* = 5). The first and second columns are the θ and ϕ coordinates (in deg) for which the radiation pattern is calculated. If the chosen type of polarization is linear (parameter *Typepolar* in the input file), then the third and the fourth columns are the normalized θ- and ϕ-components of the electric field, respectively. If the chosen type of polarization is circular, then the third and the fourth columns are the normalized right-hand circular polarization (RHCP) and left-hand circular polarization (LHCP) components of the electric field, respectively.

pat-el.dat   The file contains the field values in the elevation plane which is defined by $\phi=Phiel$ (the value of *Phiel* is defined in the input file). The input values of variables *Thetamin*, *Thetamax* and *Ntheta* determine the θ values in the elevation plane for which the radiation pattern is calculated. The field values are normalized with the field value with coordinates *Theta0* and *Phi0* that are defined in the input file (the exception is for *Nmode* = 0 and *Nmode* = 5). The first and second columns are the θ and ϕ coordinates (in deg) for which the radiation pattern is calculated. If the chosen type of polarization is linear (parameter *Typepolar* in the input file), then the third and the fourth columns are the normalized θ- and ϕ -components of the electric field, respectively. If the chosen type of polarization is circular, then the third and the fourth columns are the normalized right-hand circular polarization (RHCP) and left-hand circular polarization (LHCP) components of the electric field, respectively.

7   CONCLUSIONS

Conclusions

We proposed a 12-month effort to develop a model for analyzing circular stacked-patch antennas mounted on a double-curved conformal structure. It was also planned to develop a computer program that would rigorously analyze spherical arrays of circular stacked patch antennas. The proposed project is a continuation of the project F61775-01-WE024 "Analysis of Curved Microstrip Antennas," sponsored by EOARD. The previously developed program enables the analysis of arrays of rectangular single-patch antennas mounted on cylindrical and spherical structures.

We have developed the program SMiSPA for analyzing arrays of circular stacked-patch antennas embedded in a spherical multilayer structure. Two types of feeding structures are considered: a coaxial probe and a microstrip transmission line. The program numerically solves the electric field integral equation by means of the moment method. The solution procedure makes use of the Fourier transform technique. Since the structure exhibits spherical symmetry, the problem is solved in the spherical coordinate system, and we have used the vector Legendre transformation in θ- and ϕ-directions. In order to reduce the needed computer time the elements of the moment method matrix are calculated in the spectral domain. Direct implementation of the spectral-domain moment method is not possible for analyzing antennas with a large radius because ratios of very large numbers need to be calculated. Therefore, we have modified the vector-Legendre transformation and introduced the normalized associated Legendre functions. Furthermore, in order to analyze patch arrays on spherical structures, an efficient way of calculating the vector Legendre transforms of displaced basis and test functions has been found.

In the first 6-month period of the project we have developed the first version of the program SMiSPA that calculates the following parameters of the spherical stacked-patch arrays:

- input impedance at each input port in the array

- mutual coupling between each two patches in the array

- radiation pattern of the array when all mutual couplings are taken into account

- radiation pattern of the array without taking mutual coupling into account (fast calculations of the radiation pattern are needed for making first design of the array).

During the second 6-month period of the project we have improved the program SMiSPA. In particular, we have:

- Investigated the optimum choice of basis and test functions.

- Improved the feed model. For that purpose we have added a special attachment mode to make the feed model more accurate.

- Developed an experimental model for testing the SMiSPA program and for investigating the properties of spherical arrays of stacked-patch antennas.

The developed program is tested by comparing the calculated results with measurements of equivalent planar antennas (notice that there are no measured results of spherical stacked-patch antennas in open scientific literature). Measurements show a large sensitivity of the resonant frequency on deviations from the spherical symmetry and on the radius of the structure. In all tested cases the agreement between calculated results and measured test data is satisfactory. We additionally plan to improve the developed experimental model to obtain better accuracy of measured data.

7 Bibliography

[1]   B. Tomasic, J. Turtle, and S. Liu, "A geodesic sphere phased array for satellite control and communication," International Union of Radio Science, XXVIIth General Assembly, Maastricht, The Netherlands, August 2002.

[2]   D. L. Sengupta, T. M. Smith, and R. W. Larson, "Radiation Characteristics of Spherical Array of Circularly Polarized Elements", *IEEE Trans. on Antennas and Propagat.*, Vol. 16, pp. 2-7, Jan. 1968.

[3]   K.M Luk, K.F. Lee and J.S. Dahele, "Analysis of the Cylindrical-Rectangular Patch Antenna", *IEEE Trans. Antennas Propagation*, Vol. AP-37, No. 2, pp. 143-147, Feb.1989.

[4]   T. M. Habashy, S. M. Ali, and J. A. Kong, "Input impedance and radiation pattern of cylindrical–rectangular and wraparound microstrip antennas," *IEEE Trans. Antennas Propagat.*, vol. AP-38, pp.722-731, May 1990.

[5]   W. Y. Tam, A. K. Lai, and K. M. Luk, "Mutual coupling between cylindrical rectangular microstrip antennas," *IEEE Trans. Antennas Propagat.*, vol. AP-43, no.8, pp.897-899, Aug. 1995.

[6]   S. Raffaelli, Z. Sipus, P.-S. Kildal, "Analysis and measurements of conformal patch array antennas on multilayer circular cylinder", accepted for publication in *IEEE Transactions on Antennas and Propagation,* 2005.

[7]   P. Slättman, A. A. Kishk, "Radiation from a linear microstrip array antenna including radome and back structure", *Microwave and Optical Technology Letters,* Vol 20, pp. 119-121, Jan. 1999.

[8]   T. Kashiva, T. Onishi nd I. Fukai, "Analysis of Microstrip Antennas on a Curved Surface Using the Conformal Grids FD-TD Method", IEEE Trans. on Antennas and Propagation, Vol.AP-42, No.3, pp. 423-427, March 1994.

[9] T.Özdemir and J.L.Volakis, "Triangular Prisms for Edge-Based Vector Finite Element Analysis of Conformal Antennas", *IEEE Trans. on Antennas and Propagation*, Vol.AP-45, No.5, pp. 788-797, May 1997.

[10] W. Y. Tam and K. M. Luk, "Resonances in spherical-circular microstrip structures of cylindrical-rectangular and wraparound microstrip antennas," *IEEE Trans. Microwave Theory Tech..*, Vol. 39, pp. 700-704, 1991.

[11] W. Y. Tam, A. K. Y. Lai, and K. M. Luk, "Input impedance of spherical microstrip antenna" *IEE Proc. - Microwaves, Antennas and Propagation*, Vol. 142, 1995, pp. 285-288.

[12] H.T. Chen and K.L. Wong, "Cross-polarization characteristics of a probe-fed spherical-circular microstrip patch antenna, " *Microwave and Optical Technology Letters*, Vol. 5, pp. 705-710, Sep. 1993.

[13] A. Lima, J. Descardeci and A. Giarola, "Circular microstrip antenna on a spherical surface," *Microwave and Optical Technology Letters*, Vol. 5, pp. 221-224, May 1992.

[14] B. Ke, and A. Kishk, "Analysis of spherical circular microstrip antennas," *IEE Proc.* part H, vol. 138, 1991, pp. 542-548.

[15] K.L. Wong, *Design of Nonplanar Microstrip Antennas and Transmission Lines*, Wiley, 1999.

[16] Z. Sipus, N. Burum, J. Bartolic, "Analysis of rectangular microstrip patch antennas on spherical structures," *Microwave and Optical Technology Letters*, Vol. 36, pp. 276-280, Feb. 2003.

[17] N.Burum, Z. Sipus, and J. Bartolic, "Mutual coupling between spherical-rectangular microstrip antennas," *Microwave and Optical Technology Letters*, Vol. 40, pp. 387–391, Mar. 2004.

[18] Z. Sipus, N. Burum, S. Skokic and P.-S. Kildal, "Analysis of spherical arrays of microstrip antennas using moment method in spectral domain," Submitted to *IEEE Trans. on Antennas and Propagation*.

[19] Z. Sipus, N. Burum and R. Zentner "Analysis of Curved Microstrip Antennas," Final report for contract F61775-01-WE024, Faculty of Electrical engineering and Computing, University of Zagreb, April 2003.

[20] Z. Sipus, P.-S. Kildal, R. Leijon, and M. Johansson, "An algorithm for calculating Green's functions for planar, circular cylindrical and spherical multilayer substrates, " *Applied Computational Electromagnetics Society Journal*, Vol. 13, pp. 243-254, 1998.

[21] E.H. Newman, and J.H. Tehan, "Analysis of microstrip array and feed network," *IEEE Trans. Antennas and Propagat.*, Vol. 33, pp. 397-403, Apr. 1985.

[22] Z. Sipus, J. Bartolic, and B. Stipetic, "An approach to microstrip patch elements and array design", *Proceedings of COST 223-ESA Workshop on Active Antennas*, ESA-ESTEC, Noordwijk, The Netherlands, 1992, pp. 3.5.1-3.5.8.

[23] Z. Sipus, J. Bartolic, and B. Stipetic, "Input impedance of rectangular patch antenna fed by microstrip line, *Electronics Letters*, Vol. 28, No. 20, pp. 1886-1888, Sep. 1992. Errata, *Electronics Letters*, Vol. 28, No. 23, pp. 2199, Nov. 1992.

[24] R.F. Harrington, *Time-harmonic electromagnetic fields*, McGraw-Hill, New York, 1961.

[25] M. Abramowitz and I. Stegun, *Handbook of mathematical functions*, Dover, New York, 1965.

[26] L.B. Felsen and N. Marcuvitz, *Radiation and scattering of waves*, Prentice-Hall, New Jersey, 1973.

[27] R. Paknys, "Evaluation of Hankel functions with complex argument and complex order," *IEEE Trans. Antennas and Propagat.*, vol. 40, pp. 569-578, May 1992.

[28] Y.T. Lo, D Soloman and W.F. Richards, "Theory and experiment of microstrip antennas," *IEEE Trans. Antennas and Propagat.*, vol. 27, pp. 137-145, Feb. 1979.

[29] A.N. Tulintseff, S.M. Ali and J.A. Kong, "Input impedance of a probe-fed stacked circular microstrip antenna," *IEEE Trans. Antennas and Propagat.*, vol. 39, pp. 381-390, March 1991.

[30] M.D. Deshpande and M.C. Bailey, "Analysis of finite arrays of circular microstrip patches," *IEEE Trans. on Antennas and Propagat.*, Vol. 37, pp. 1355-1360, Nov. 1989.

[31] R.F. Harrington, *Time-harmonic electromagnetic waves*, McGraw Hill, New York, 1961.

[32] A. Lima, J. Descardeci and A. Giarola, "Circular microstrip antenna on a spherical surface," *Microwave and Optical Technology Letters*, Vol. 5, pp. 221-224, May 1992.

[33] E. Lier and K. R. Jakobsen, "Rectangular microstrip patch antennas with infinite and finite ground plane dimensions," *IEEE Trans. Antennas Propagat.*, Vol. 31, pp. 978-984, Nov.1983.